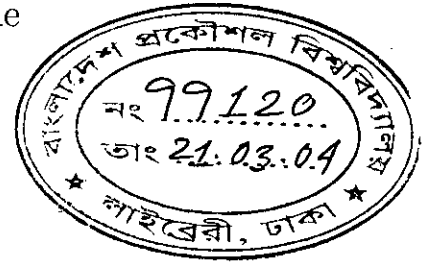# Design of Delayless Subband Echo Cancelers using Parallel Kalman Filters

by

Mohammad Zulhasnine

A thesis submitted to the Department of Electrical and Electronic Engineering of
Bangladesh University of Engineering and Technology
in partial fulfillment of the requirements for the degree of
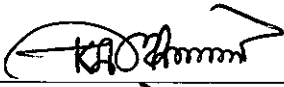MASTER OF SCIENCE IN ELECTRICAL AND ELECTRONIC ENGINEERING

DEPARTMENT OF ELECTRICAL AND ELECTRONIC ENGINEERING
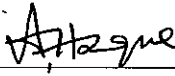BANGLADESH UNIVERSITY OF ENGINEERING AND TECHNOLOGY
February 2004

The thesis titled **"Design of Delayless Subband Echo Cancelers using Parallel Kalman Filters"** submitted by Mohammad Zulhasnine Roll No.: 040206223P, Session: April, 2002 has been accepted as satisfactory in partial fulfillment of the requirements for the degree of **Master of Science in Electrical and Electronic Engineering** on February 26, 2004.

BOARD OF EXAMINERS

1. _____   **Chairman**
(Dr. Md. Kamrul Hasan)
Associate Professor
Department of Electrical and
Electronic Engineering, BUET,
Dhaka-1000, Bangladesh

2. _____   **Member**
(Dr. Md. Aynal Haque)
Associate Professor
Department of Electrical and
Electronic Engineering, BUET,
Dhaka-1000, Bangladesh

3. _____   **Member**
(Dr. Mohammad Ali Choudhury)   (Ex-officio)
Professor and Head
Department of Electrical and
Electronic Engineering, BUET,
Dhaka-1000, Bangladesh

4. _____   **Member**
(Dr. Farruk Ahmed)   (External)
Professor
Department of Computer Science
and Engineering,
North South University,
Dhaka-1213, Bangladesh

Declaration

It is hereby declared that this thesis or any part of it has not been submitted elsewhere for the award of any degree or diploma.

Signature of the candidate

Zulhasnine

(Mohammad Zulhasnine)

Dedication

To my beloved students at Jahangirnagar University.

Acknowledgements

I wish to express my deepest gratitude to Dr. Md. Kamrul Hasan, my supervisor, for his many suggestions and constant supports during this thesis work. His breadth of knowledge has never ceased to amaze me.

I am also grateful to Professor M. Rezwan Khan, my undergrad thesis supervisor, and Dr. Md. Zulkernine, my brother, both of whom actually suggested me to work under Dr. Md. Kamrul Hasan.

I would like to thank Dr. Mohammad Ali Choudhuri, Dr. Md. Aynal Haque and Dr. Farruk Ahmed for serving on my committee. I would also like to thank the researchers of our DSP group for their help and patience during the course of my work.

Finally, I would like to thank my entire family and all my friends for supporting and standing by me through the years.

Contents

List of Tables

List of Figures

List of Principal Symbols

t	Discrete time index
$x(t)$	Far-end speech signal
$y(t)$	The microphone signal
$d(t)$	Echo signal to the microphone
$e(t)$	Wideband error
$s(t)$	Near-end speech signal
$n(t)$	Ambient noise signal
$w(t)$	Echo path impulse response
$\hat{w}(t)$	Estimated echo path impulse response
N	Number of data points
$\hat{\boldsymbol{w}}_i$	Estimated weight vector of i-th part filter
$\hat{\boldsymbol{x}}_i$	i-th part reference signal
μ	Step size parameter for LMS algorithm
$\tilde{\mu}$	Adaptation constant for NLMS algorithm
J	Number of parallel filter
P	Number of filter taps in each part
σ_n^2	Variance of measurement noise
D	Decimation factor
I	Interpolation factor or identity matrix
$h_0(n)$	Impulse response of a lowpass prototype filter
$H_m(z)$	Transfer function of the m-th band analysis filter
$F_m(z)$	Transfer function of the m-th band synthesis filter
$\boldsymbol{w}_m$	N/D subband weight vector
$\hat{\boldsymbol{w}}_m(t)$	Estimated subband weight vector at time t
$x_m(t)$	The m-th subband reference signal
$\boldsymbol{x}_m(t)$	N/D most recent reference signals weight vector
$w_{(m,i)}$	The i-th coefficient of the m-th subband

$\hat{d}_m(t)$ Estimated echo of the m-th subband at time t

$e_m(t)$ The m-th subband local error signal

$E[\cdot]$ Expectation operator

$u(t)$ Zero-mean white noise

Abbreviations

AECs	Acoustic Echo Cancelers
CL	Close Loop
DSAEC	Delayless Subband Acoustic Echo Canceler
DTD	Double Talk Detector
ECFs	Echo Cancellation Filters
ERLE	Echo Return Loss Enhancement
KF	Kalman Filter
OL	Open Loop
PKFs	Parallel Kalman Filters
PSTN	Public-switched Telephone Network
FES	Far End Speaker
NES	Near End Speaker
NLMS	Normalized LMS
PNLMS	Parallel NLMS
TIC	Time of Initial Convergence

Abstract

The key concern of this thesis work is to design an Acoustic Echo Canceler (AEC) which meets the requirements of fast convergence rate and less computational burden. Adaptive filters are used for real time identification of the impulse response of an acoustic echo path. The length of the acoustic echo path impulse responses (often several hundred milliseconds) leads to the adaptive filters with very large filter taps. Delayless subband filters offer computational savings, as well as faster convergence over the correspondent fullband adaptive filters. However, conventional delayless subband filters use LMS or normalized LMS (NLMS) algorithm for coefficient adaptations in the subband domain. Application areas such as hands-free communication in cars, mobile communications and video conferencing have created further demands for high-quality acoustic echo cancellation in terms of Echo Return Loss Enhancement (ERLE). It is known that Kalman filter (KF) algorithm shows better convergence rate than the conventional LMS and NLMS algorithm but with the cost paid in computational complexity. In this work we propose a new design method using parallel Kalman filters (PKFs) in the subband domain which require less computations. Incorporation of parallel architecture in each subband provides a flexibility in trade-off between the number of subbands and parallel filters in each subband for optimum performance of subband adaptive filters. The simulation results show that proposed AEC performs better both in terms of ERLE and computational complexity than that of the LMS and NLMS algorithms.
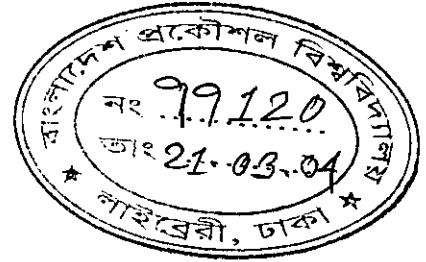
Chapter 1

Introduction

1.1 Echo Cancellation: Background

Echo may incur whenever we talk or make sound. If the delay between the speech and its echo is short, the echo is unnoticeable and referred to as *reverberation*. On the other hand, if the delay exceeds a few tens of milliseconds, the echo is distinctly noticeable [1]. Echo is widely employed in sonar and radar for the purpose of detection and exploration. But in telecommunication, echo degrades the voice quality and echo cancellation is a vital part to meet acceptable quality of service.

There are two types of echo in communication systems: telephone line hybrid echo and acoustic echo. Hybrid echo can be generated electrically, due to the impedance mismatch at points along the transmission medium of the public-switch telephone network (PSTN). As the cost of leasing a *four-wire* telephone circuit is too high, a *two-wire* circuit is used to connect a subscriber to the main four-wire telephone channels at the central office [2]. A device, named as *hybrid*, provides the interface between a two-wire and a four-wire circuit as shown in Fig. 1.1. As a hybrid device is shared among several subscribers, it is difficult to achieve impedance matching. Due to this impedance mismatch between the hybrid and the telephone channel, the input port becomes coupled to the output port, causing "echo". Such echo is called telephone line hybrid echo.

On the other hand, the acoustic echo problem arises, whenever there is acoustic coupling between a loudspeaker and a microphone, such as in hands-free phones, mobile phones, and teleconference systems. In these systems, the microphone signal picks up the far-end speech after it has traveled through the

1
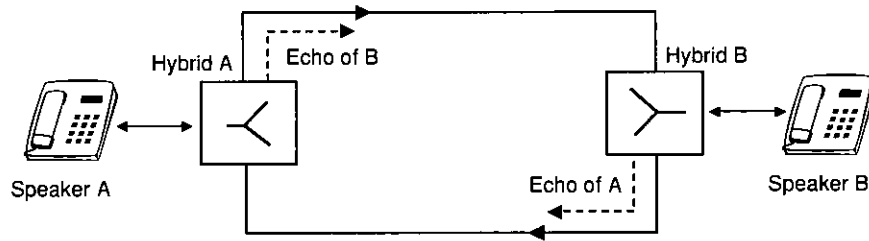
Fig. 1.1: Basic 2/4-wire interconnection scheme.

acoustic medium, and consequently, echo is heard at the far end. The acoustic coupling between the loudspeaker and the microphone may even make the system unstable and produce a *howling* [1].

Echo control methods are usually divided into two categories: echo cancellation and echo suppression. Telephone companies employ "echo suppressor" which is primarily a switch that lets the speech signal pass through during the speech-active periods and attenuates the line echo during the speech-inactive periods. This traditional voice-activated switched-loss echo suppressors meet the demand only for terrestrial communication and fail to perform satisfactorily in systems with extremely long round trip delay [3]. Adaptive echo canceler has been introduced which is effective with both short and long time delays. The adaptive filter creates a replica of the echo using the signal in the received path and subtracts it from the signal in the transmitter path as indicated in Fig. 1.2.
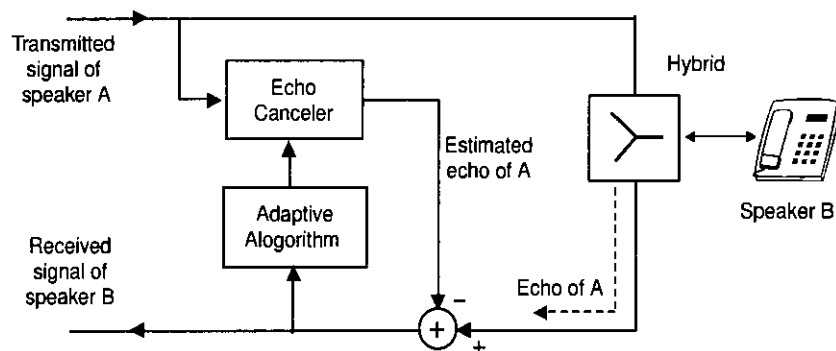
Fig. 1.2: Adaptive echo canceler in landline telecommunication system.

Comparing typical impulse responses of these two kinds of echo paths, it becomes obvious that acoustic echo cancellation is far more challenging task than the line echo cancellation. [4]. The impulse response of the acoustic echo path is usually several times longer than that of line echo path and is the major topic of this thesis work.

Even though echo cancellation belongs to the traditional problems of signal processing, it is still an active field of research. New attention has been drawn to the subject with the advent of digital wireless communication systems for the following reasons. The echo problem becomes severe because of longer signal path delays produced by sophisticated speech coding algorithms. The effect of echo is worst for telephone networks involving geostationary satellite circuits, where the echo delay is about 540 ms [2]. Also, there are appreciable delays of up to 200 ms inherent in digital mobile phones, which make any echo quite noticeable. For this reason the employment of echo cancelers in PSTN and mobile switching centres is a mandatory. The use of hands-free communication in cars, computer applications and video conferencing has also created a demand for high-quality acoustic echo cancellation. Thus, acoustic echo cancellation is an important aspect of the design of modern telecommunication systems such as conventional wireline telephones, hands-free phones, cellular mobile phones, or teleconference systems [5].

1.2   Literature Review

Acoustic echo cancellation is a long-lasting challenge since its invention in the 1960s at Bell Labs [6]-[8]. In recent years, adaptive filters are used in many applications such as adaptive modeling, adaptive noise cancellation, and adaptive signal enhancement [9], [10]. Adaptive filter is also used for real time identification of the impulse response of an acoustic echo path. The length of the acoustic echo path impulse responses (often several hundred milliseconds) leads to the adaptive filters with very large filter taps. In some applications, such as acoustic echo cancellation and active noise control, where the number of filter taps to be estimated is large, computational complexity is a burden. Moreover, adaptive filters with many taps suffer from slow convergence, especially, if the eigenvalues of the underlying correlation matrix of the input signal are widely spread [10]. One approach for reducing the computational complexity of long adaptive filters is to use block signal processing methods [11]-[15]. The major disadvantage of such approaches is a long block delay associated with the adaptive weight update. The use of parallel Kalman filters (PKFs) in the time-domain is another approach for improving the convergence rate [16].

Recently, subband techniques have been developed for adaptive filters to re-

duce the computational complexity and to improve the convergence rate [17]. This technique has been applied to the acoustic echo cancellation problem in order to overcome the problems of slow convergence due to spectrally dynamic input and high computational costs associated with a single, long adaptive filter [17]-[30]. As both the number of taps and weight update rate can be decimated in each subband, computational burden is reduced by approximately the number of subbands. Faster convergence is achieved due to the reduction of spectral dynamic range in each subband. The major disadvantages of subband structures, however, are aliasing due to downsampling [21] and the transmission delay introduced into the signal path due to the bandpass filters used for deriving the subband signals. To avoid signal path delay, Morgan and Thi reported a new type of delayless subband adaptive filter architecture in which the adaptive weights are computed in subbands but collectively transformed into an equivalent set of wideband filter coefficients [30]. An additional benefit accrues through a significant reduction of aliasing effect. Commonly, subband implementations employ LMS or normalised LMS (NLMS) algorithm for its coefficients adaptation in each subband. Although the estimation algorithm of adaptive filters using such a method is simple, they are weak for the case of nonwhite input signal [16].

The increasing use of teleconference systems and video conferencing where the AEC plays a central role, has further led to the requirement of faster and better performing adaptive filter. In this work, we modify the delayless subband adaptive filter [30] by replacing the conventional NLMS/KF algorithm with PKFs for coefficients adaptation in each subband. Incorporation of parallel architecture in each subband provides a flexibility in trade-off between the number of subbands and parallel filters in each subband for optimum performance of subband adaptive filters. A design method for PKFs in the subband domain is proposed. Computational complexity and experimental results comparing the performance of such adaptive subband parallel NLMS (PNLMS) and PKFs are shown.

1.3 Thesis Overview

This section is intended to give a short overview of the thesis, by describing the outline of each chapter. In Chapter 2 the acoustic echo problem is introduced, and its traditional solution, AEC, is discussed. We also discuss parallel LMS/NLMS

and PKFs algorithms in time domain for estimating the acoustic echo path of an AEC.

Chapter 3 starts by conventional delayless subband AEC. Polyphase FFT technique is also presented to derive complex subband signals. Then a modified delayless subband AEC is presented where PKFs are employed in the subband domain for coefficients adaptation. These modification gives better performance and convergence rates when using speech signals for identification of the acoustic channel. The chapter ends with an analysis of the computational complexity of AECs.

In Chapter 4, simulation results are presented along with figures and remarks. Comparison with the results of other methods is presented to show the superiority of the proposed method specially when the acoustic echo path is long.

Chapter 5 contains the conclusions of the work and suggests future work.

In Appendix, uniform filter bank and its polyphase implementation are presented in detail.

Chapter 2

Acoustic Echo Cancellation

The general concept of an echo canceler is described. Parallel LMS/NLMS and PKFs algorithms are presented as a solution to acoustic echo problem.

2.1 The Acoustic Echo Problem

The acoustic echo problem arises, whenever there is acoustic coupling between a loudspeaker and a microphone. Fig. 2.1 illustrates a system where a far-end speaker (FES) is impaired by the echo of his own voice which superposes on the near-end speaker's (NES) end. Because of the acoustic transmission path from
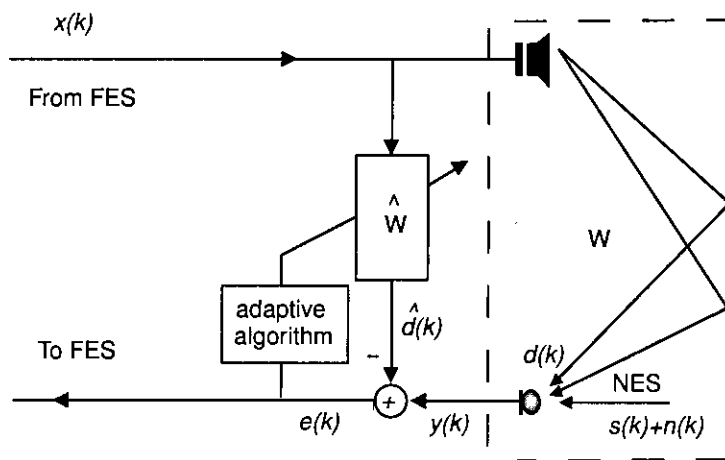
Fig. 2.1: The acoustic echo problem.

the loudspeaker to the microphone, the speech, $x(t)$ from the FES, feeds back to the microphone as an echo signal, $d(t)$. Assuming that acoustic channel is linear, the echo signal received on the microphone is the result of the convolution

6

between the signal present on the loud speaker $x(t)$ and $w(t)$, that is

$$
\begin{aligned}
d(t) &= w_0 x(t) + w_1 x(t-1) + ... + w_{N-1} x(t - N + 1) \\
&= \boldsymbol{w}^T \boldsymbol{x}(t)
\end{aligned}
\tag{2.1}
$$

Here, $\boldsymbol{w} = [w_0, w_1, ..., w_{N-1}]^T$ is the echo path impulse response of finite length[1] N, and $\boldsymbol{x}(t) = [x(t), x(t-1), ..., x(t - N + 1)]$ is a vector comprising of N most recent loudspeaker signal samples, and t denotes a discrete time index.

The microphone signal $y(t)$ is transmitted back to the far-end speaker as the sum of the echo signal $d(t)$, near-end speech $s(t)$, and the ambient noise $n(t)$,

$$
\begin{aligned}
y(t) &= d(t) + s(t) + n(t) \\
&= \boldsymbol{w}^T \boldsymbol{x}(t) + s(t) + n(t)
\end{aligned}
\tag{2.2}
$$

Eq. (2.2) will be considered as an acoustic model [31]. The echo signal $d(t)$ needs to be removed from the microphone signal $y(t)$ for echo-free conversation.

2.2 Acoustic Echo Cancellation

We will confine on single-channel AEC, with one loudspeaker and one microphone. To cancel the echo signal $d(t)$ from the microphone signal $y(t)$, AEC estimates $d(t)$ using an approximation algorithm and subtracts the estimated echo signal, $\hat{d}(t)$ from $y(t)$. The estimation error signal $e(t)$ is expressed as

$$
\begin{aligned}
e(t) &= y(t) - \hat{d}(t) \\
&= [d(t) - \hat{d}(t)] + s(t) + n(t).
\end{aligned}
\tag{2.3}
$$

The error signal is estimated in a mean square sense. The MSE is defined as

$$
\begin{aligned}
E\{[d(t) - \hat{d}(t)]^2\} &= E\{[e(t) - s(t) - n(t)]^2\} \\
&= E\{e^2(t)\} + E\{s^2(t)\} + E\{n^2(t)\} + 2E\{s(t)n(t)\}
\end{aligned}
$$
$$
-2E\{e(t)[s(t) + n(t)]\}.
\tag{2.4}
$$

We simplify Eq. (2.4) by assuming that $e(t)$, $s(t)$, and $n(t)$ are uncorrelated,

$$
E\{[d(t) - \hat{d}(t)]^2\} = E\{e^2(t)\} + E\{s^2(t)\} + E\{n^2(t)\}.
\tag{2.5}
$$

---

[1]The number of filter parameters could be reduced by modeling the acoustic echo path with an infinite impulse response (IIR) filter. However, due to the practical difficulties associated with the adaptation and stable operation, the IIR filter still has few degrees of freedom [4].

Neither $s(t)$ nor $n(t)$ depends on $\hat{d}(t)$, minimizing $E\{[d(t) - \hat{d}(t)]^2\}$ is thus equivalent to minimizing $E\{e(t)^2\}$. AEC creates the estimated echo signal $\hat{d}(t)$ based on the identification of the acoustic channel $w(t)$ between the loudspeaker and the microphone,

$$\hat{d}(t) = \hat{w}^T x(t). \tag{2.6}$$

As the echo path, $w(t)$ changes over time due to moving objects or change in temperatures, the coefficients must therefore be estimated using an adaptive algorithm. An adaptive algorithm is therefore an essential part of AEC. In any conversation, usually the talkers do not speak simultaneously, and hence speech and echo are seldom present on a line at the same time. When the NES is quiet $[s(t) = 0]$ and the level of the ambient noise, $n(t)$ is low $[n(t) = 0]$, the adaptation process simplifies as

$$e(t) = d(t) - \hat{d}(t). \tag{2.7}$$

Then the adaptive filter can converge to the true echo path impulse response $w(t)$. During double-talk[2], the near-end signal $s(t)$ is acting as high-level uncorrelated noise, leading to insufficient echo cancellation. Therefore, to avoid divergence, "real world" acoustic echo controllers typically include in addition to the echo cancellation filters (ECFs), a double talk detector (DTD) for freezing filter coefficients during the presence of NES speech. The echo only period is detected by various DTDs based on cross-correlating properties [34]-[35][3]. An AEC is shown in Fig. 2.1 which produces a synthesized echo from the far-end speech with an adaptive filter fine tuned to the echo path, and subtracts this echo from the microphone signal.

2.3 Parallel Estimation of Acoustic Echo Path in Time Domain

As mentioned in the preceding section, an adaptive filter is required to model the unknown echo path w which is not only time-varying but also different for

---

[2] *Double talk* (DT) mode corresponds to the simultaneous presence of local speech and echo (local and remote speakers speaking simultaneously), and *single-talk* (ST) mode corresponds to the presence of echo only.

[3] *Double talk* aspects are not investigated in details. A theoretical study of those aspects would be certainly very complex.

each network path. However, as the parameters to be estimated is large in acoustic echo cancellation, real time processing becomes difficult using conventional LMS/NLMS and KF methods because of large computational burden. As a solution to this problem, PNLMS and KF methods for coefficients adaptation are presented here.

The adaptive weights $\hat{w}$, to be estimated, are divided into J parts, namely Part 1, Part 2,..., Part J. In the z-domain $\hat{w}$ can be represented as

$$\hat{W}(z) = \sum_{i=0}^{N-1} \hat{w}_i z^{-i} \qquad (2.8)$$

If we divide the adaptive weights into J parts, then $\hat{w}$ can be expressed as

$$\hat{w} = [\hat{w}_1^T, \hat{w}_2^T, ..., \hat{w}_J^T]^T. \qquad (2.9)$$

The adaptive weights of each part are given by

$$\hat{w}_i = [\hat{w}_{P(i-1)}, \hat{w}_{P(i-1)+1}, ..., \hat{w}_{Pi-1}]^T, \quad i = 1, 2, ..., J \qquad (2.10)$$

where $P = N/J$ is the number of elements of each part. In Eq. (2.10), $\hat{w}_{P(i-1)}$ denotes the $P * (i-1)$-th coefficient. If necessary some zeros should be added to the J-th part of the adaptive weights so as to make $P = N/J$ an integer. We divide the reference signal $x(t)$ into J parts expressed as

$$x(t) = [x_1^T(t), x_2^T(t), ..., x_J^T(t)]^T \qquad (2.11)$$

Here, $x_i(t)$ represents i-th part reference signals defined as

$$x_i(t) = [x(t - P(i-1)), x(t - (P(i-1)+1)), ..., x(t - (P(i-1)+P-1))] \qquad (2.12)$$

The J segments of the impulse response described in Eq. (2.10) are estimated using J number of parallel filters as indicated in Fig 2.2. The total estimated echo signal $\hat{d}(t)$ at time t of the J pieces of filters in parallel is given by

$$\hat{d}(t) = \sum_{i=1}^{J} \hat{d}_i(t) = \sum_{i=1}^{J} \hat{w}_i^H(t-1) x_i(t). \qquad (2.13)$$

The superscript H indicates *Hermitian transposition*. Note that the order of the resultant filter is JP.

9
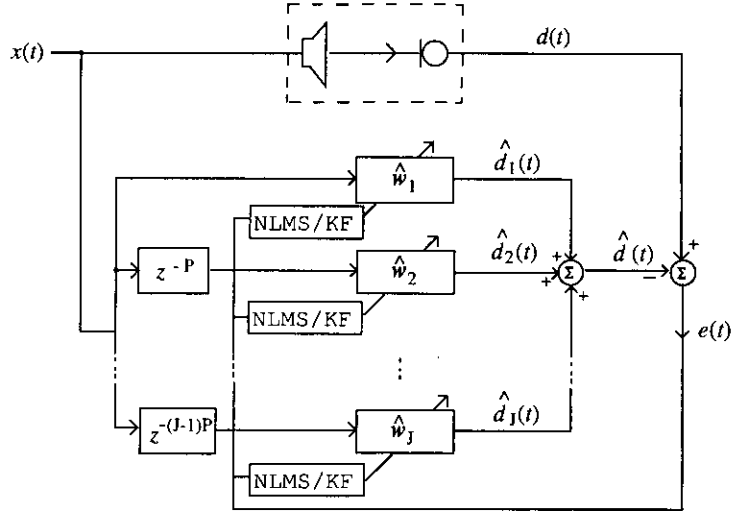
Fig. 2.2: Echo canceler using parallel adaptive filter.

2.3.1 Estimation using Parallel LMS/NLMS Methods

To obtain the optimal solution of the coefficients of the resultant filter, the total error $e(t)$ is used for estimation of the parameters. See Eq. (2.13). The LMS estimation algorithm of the i-th part:

$$e(t) = d(t) - \sum_{i=1}^{J} \hat{w}_i^H(t-1)x_i(t), \qquad (2.14)$$

$$\hat{w}_i(t) = \hat{w}_i(t-1) + \mu x_i(t)e^*(t) \qquad (2.15)$$

The range of step size parameter, μ, is given by the equation:

$$0 < \mu < \frac{2}{PS_{max}},$$

where S_{max} is the maximum value of the power spectral density of the reference signal $x(t)$. The superscript $'*'$ denotes complex conjugation.

The NLMS estimation algorithm of the i-th part:

$$e(t) = d(t) - \sum_{i=1}^{J} \hat{w}_i^H(t-1)x_i(t), \qquad (2.16)$$

$$\hat{w}_i(t) = \hat{w}_i(t-1) + \frac{\tilde{\mu}}{\| x(t) \|^2} x_i(t)e^*(t) \qquad (2.17)$$

where $\tilde{\mu}$ is the adaptation constant given by:

$$0 < \tilde{\mu} < 2\frac{E[|\, x_i(t)\,|^2]D(t)}{E[|\, e(t)\,|^2]},$$

$E[|\, e(t)\,|^2]$ is error signal power, $E[|\, x_i(t)\,|^2]$ is reference signal power, and $D(t)$ is mean square deviation. Note that in Eq. (2.17), adaptive constant is normalized

using $\parallel \boldsymbol{x}(t) \parallel^2$ instead of $\parallel \boldsymbol{x}_i(t) \parallel^2$ for achieving better convergence rate. Because of this modification, adaptive filter using PNLMS algorithm performs exactly same to the adaptive filter using NLMS algorithm. Numerical difficulties may arise if the squared norm $\parallel \boldsymbol{x}(t) \parallel^2 = 0$. To overcome this problem, Eq. (2.17) is modified as

$$\hat{\boldsymbol{w}}_i(t) = \hat{\boldsymbol{w}}_i(t-1) + \frac{\tilde{\mu}}{\delta + \parallel \boldsymbol{x}(t) \parallel^2} \boldsymbol{x}_i(t) e^*(t), \qquad (2.18)$$

where $\delta > 0$.

It is well-known that the NLMS algorithm exhibit a rate of convergence that is potentially faster than that of the standard LMS algorithm for both correlated and uncorrelated input data [36]. For both LMS and NLMS algorithms, $\hat{\boldsymbol{w}}_i(0) = \boldsymbol{0}$, as prior knowledge of the tap vector is unknown.

The computational complexity of the PNLMS algorithm in the time domain is approximately $2N/p_{std}$ where p_{std} denotes the number of parallel section for time domain approach.

2.3.2 Estimation using Parallel Kalman Method

The optimal algorithm of PKF in time domain for the i-th part is:

$$\boldsymbol{k}_i(t) = \frac{\boldsymbol{Q}_i(t-1)\boldsymbol{x}_i(t)}{\sigma_n^2 + \sum_{l=1}^{J} \boldsymbol{x}_l^H(t)\boldsymbol{Q}_l(t-1)\boldsymbol{x}_l(t)} \qquad (2.19)$$

$$e(t) = d(t) - \sum_{i=1}^{J} \hat{\boldsymbol{w}}_i^H(t-1)\boldsymbol{x}_i(t) \qquad (2.20)$$

$$\hat{\boldsymbol{w}}_i(t) = \hat{\boldsymbol{w}}_i(t-1) + \boldsymbol{k}_i(t)e^*(t) \qquad (2.21)$$

$$\boldsymbol{Q}_i(t) = [\boldsymbol{I} - \boldsymbol{k}_i(t)\boldsymbol{x}_i^H(t)]\boldsymbol{Q}_i(t-1) \qquad (2.22)$$

Here $i = 1, 2, ..., J$. For initialization,

$$\boldsymbol{Q}_i(0) = \beta_i \boldsymbol{I}; \quad \beta_i > 0 \qquad (2.23)$$

$$\hat{\boldsymbol{w}}_i(0) = \boldsymbol{0}, \qquad (2.24)$$

where σ_n^2 is the variance of measurement noise and $\boldsymbol{I}$ is the unit matrix of dimension $P \times P$. σ_n^2 is assumed to be 1 which indicates that this method can be used even when σ_n^2 is unknown [16]. The β_i denotes the degree of uncertainty of $\hat{\boldsymbol{w}}_i(0)$, which is taken to be large when initial filter taps are unknown.

It is to be noted that the computational complexity of the PKFs in time domain is $(8N/p_{std})^2 + 16N/p_{std}$ [16].

Chapter 3

Delayless Subband Acoustic Echo Canceler

Conventional delayless subband AEC is presented first. Modification is suggested to this AEC by introducing PKFs in the subband domain which provides improved performance both in terms of ERLE and computational complexity. Computational complexity is addressed at the end.

3.1 Conventional Delayless Subband Acoustic Echo Canceler

With the high number of adaptive filter weights required, popular adaptive filters based on LMS/NLMS/KF algorithms in time domain become very computationally expensive and exhibit slow convergence. One possibility to combat these problems is the use of adaptive algorithms, together with multirate techniques, to split the full-band problem into smaller subband problems. Fig. 3.1 shows the architecture of the delayless subband AEC (DSAEC) with conventional NLMS/KF adaptation [30]. The coefficients in each band, can be calculated either by employing the error signal $e(t)$ (closed loop case) or the microphone input signal $d(t)$ (open loop case). Here only open loop case is presented. Adaptive weights are computed in the subband domain using the complex LMS/NLMS/KF algorithm and then collectively transformed into frequency domain using the FFT, appropriately stacked, and inverse transformed to obtain the wideband filter coefficients, thereby eliminating any delay associated with the cancellation signal[1]. For N

---

[1]The complex subband decompositions leads to a straightforward method of eliminating the filter bank delay. Since the adaptive filter coefficients are determined inside the subbands
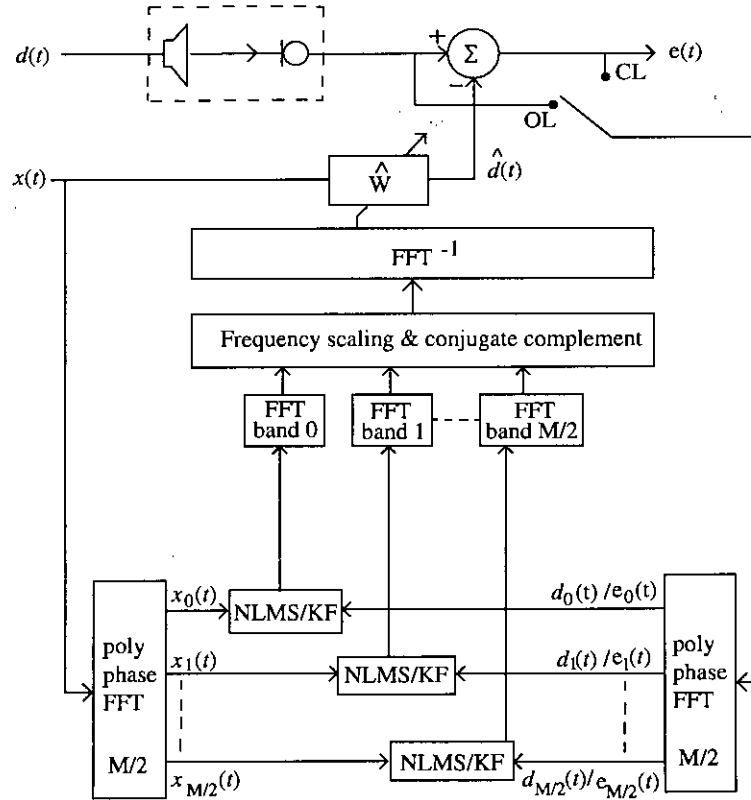
Fig. 3.1: Conventional delayless subband echo canceler; position OL for open loop and position CL for close loop operation.

wideband adaptive weights and a decimation factor D, there are $N/D = 2N/M$ adaptive weights for each subband. Let $\boldsymbol{w}_m$ is a vector of N/D subband weights, $\boldsymbol{x}_m(t) \equiv [x(t), x(t-D), ..., x(t-N+D)]^T$ is a vector comprising the N/D most recent signals of the subband filter reference signal. The adaptive weights of the m-th subband are given by

$$\boldsymbol{w}_m = [w_{(m,1)}, w_{(m,2)}, ..., w_{(m,N/D-1)}]^T \tag{3.1}$$

In Eq. (3.1), $w_{(m,i)}$ denotes the i-th coefficient of the m-th subband. Estimated echo of the m-th subband, $\hat{d}_m(t)$ at time t

$$\hat{d}_m(t) = \hat{\boldsymbol{w}}_m^H(t-1)\boldsymbol{x}_m(t) \tag{3.2}$$

whereas desired output $\hat{d}(t)$ is computed outside the subbands by convolving the reference signal, the signal path thus doesn't experience any delay induced by the analysis/synthesis filter bank. Note that synthesis filter bank is not required since the desired signal is not computed in the subbands.

where $\hat{w}_m(t)$ denotes the estimated weight vector. The m-th subband local error signal is defined as

$$e_m(t) = d_m(t) - \hat{d}_m(t) \tag{3.3}$$

As the wideband error is not fed back to the subband weight calculation, this can be thought of open loop version[2].

3.1.1 Subband Decomposition of Signals

Multirate digital processing systems employ multiple sampling rates in the processing of digital signals. Subband decomposition is a special technique of multiresolution signal decomposition. The basic idea is to divide the frequency band into a set of uncorrelated frequency bands, usually non-overlapping, by filtering [38] .

There are several ways to derive complex subband signals [32]-[33]. In this work, the reference signal $x(t)$, and the disturbance signal $d(t)$ are divided into several subband signals by using an analysis filter bank consisting M contiguous filters $H_m(z)$, $m = 0, 1, ..., M-1$ as indicated in Fig. 3.2. The transfer function $H_m(z)$ in the z-domain can be expressed as

$$H_m(z) = \sum_{k=0}^{\infty} h_m(k)z^{-k} = \sum_{k=0}^{\infty} h_0(k)e^{\frac{j2\pi mk}{M}}z^{-k}, \quad m = 0, 1, ..., M-1 \tag{3.4}$$

It is to be noted that $H_m(z)$ is derived from a lowpass prototype filter $H_0(z)$,
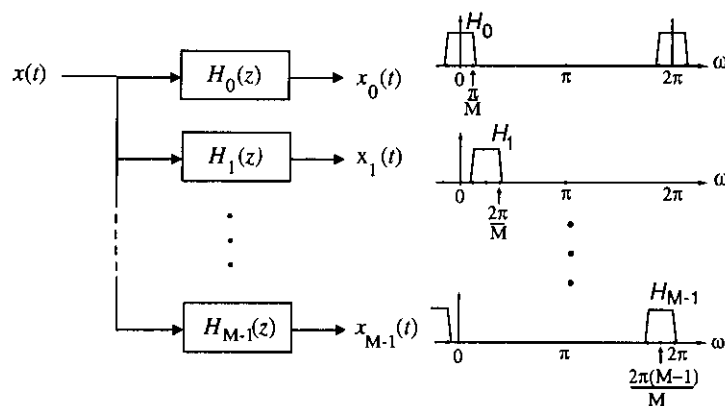

Fig. 3.2: Analysis filter bank for subband decompositions.

---

[2]The closed-loop version converges somewhat slower initially because of the delay in the wideband filter update.

14

where $H_m(z) = H_0(zW_M^m)$ for $m = 0, 1, ..., M-1$ and the details of which are described in Appendix A. Now, the m-th subband reference signal is mathematically expressed as

$$x_m(t) = \sum_{k=0}^{\infty} h_0(k)e^{\frac{j2\pi mk}{M}}x(t-k), \quad t = 0, 1, 2, ... \tag{3.5}$$

Let $a_k = h_0(k)$ are the coefficients of a $K(= LM)$ point prototype filter, where L is an integer. Eq. (3.5), the above equation can be rewritten as

$$x_m(t) = \sum_{k=0}^{K-1} a_k e^{\frac{j2\pi mk}{M}}x(t-k) \tag{3.6}$$

$$= \sum_{n=0}^{M-1} e^{\frac{j2\pi mk}{M}} \sum_{l=0}^{L-1} a_{n+l}x(t-k). \tag{3.7}$$

It is obvious that Eq. (3.6) expresses the convolution of the frequency-shifted prototype filter with the filtered reference signal to obtain a single sideband reference signal. And the expression in Eq. (3.7) shows how the inverse FFT comes into play. The signal $d(t)$ is also decomposed in the similar way to obtain $d_m(t)$ corresponding to the m-th subband.

Since the output of the lowpass filter is relatively narrow in bandwidth, the signal can be decimated[3] by a factor $D \leq M$. The resulting decimated output signal can be expressed as

$$x_m(t) = \sum_{k=0}^{\infty} h_0(k)e^{\frac{j2\pi mk}{M}}x(tD-k), \quad t = 0, 1, 2, ... \tag{3.8}$$

Or, simply

$$x_m(t) = \sum_{k=0}^{\infty} h_0(k)e^{\frac{j2\pi mk}{M}}x(t-k), \quad t = D, 2D, 3D, ... \tag{3.9}$$

The *subsampler*, or *down-sampler* is represented by a square enclosing a downward arrow in Fig 3.3. In order to reduce the effects of aliasing caused by downsampling, oversampled $(D < M)$ schemes are often used instead of critically-sampled $(D = M)$ schemes which require additional adaptive cross filters to compensate for the effects of aliasing. The oversampling factor for this design is $M/D = 2$.

---

[3]The process of reducing the sampling rate by a integer factor D (downsampling by D) is called *decimation*. The process of increasing the sampling rate by a factor I (upsampling by I) is called *interpolation*.
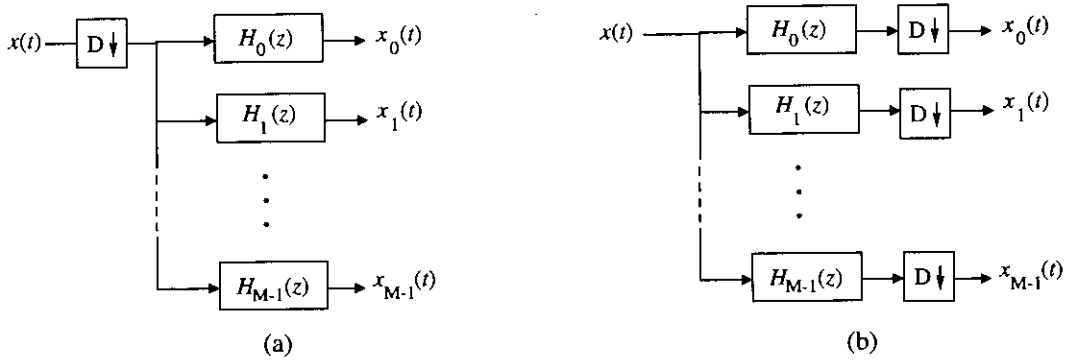
Fig. 3.3: The M-channel oversampled digital filter bank with uniform decimation ratio D.

The time compression implicit in Eq. (3.9) is accomplished by stretching in frequency domain so that the interval from 0 to π/M now covers the band from 0 to π. It should be evident that the process of discarding sample can lead to a loss of information. In frequency domain this is the aliasing effect [38].

As the bandwidth in each subband is reduced, the sampling frequency for each subband filter can be lowered. Consequently adaptive filters need fewer taps in comparison to fullband solutions to cover the same time interval and are updated at a lower rate. This leads to a significant deduction of computational complexity.

Another technique which can be employed to extract complex subband signals is the polyphase FFT technique described in [32]. This technique realizes M contiguous single-sideband bandpass filters with their outputs downsampled by a factor $D = M/2$ to produce M complex subband signals.

Fig. 3.4: Polyphase implementation of digital filter bank with uniform decimation ratio D.

Also no band shifting is necessary due to regular structure; even subbands are centered at dc while odd subbands are centered at one half of the decimated

sampling frequency [30]. Since for real signals, the wideband filter coefficient are real, only half of the subbands need to be processed.

3.1.2 Coefficient Adaptation Methods

To obtain the optimal solution of the coefficients of the resultant filter, the subband local error $e_m(t)$ is used to estimate the parameters.

KF algorithm:
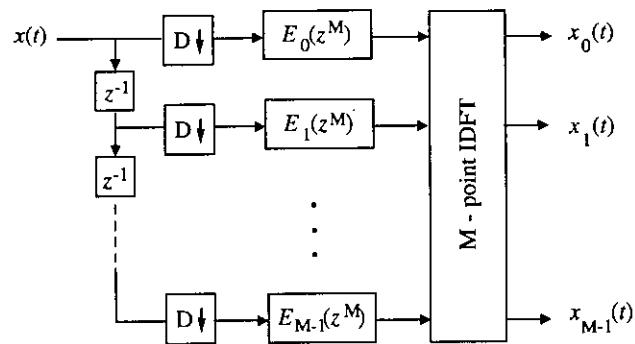
The optimal KF algorithm for the m-th subband is obtained as shown in the following:

$$k_m(t) = \frac{Q_m(t-1)x_m(t)}{\sigma_n^2 + x_m^H(t)Q_m(t-1)x_m(t)}, \tag{3.10}$$

$$e_m(t) = d_m(t) - \hat{w}_m^H(t-1)x_m(t), \tag{3.11}$$

$$\hat{w}_m(t) = \hat{w}_m(t-1) + k_m(t)e_m^*(t) \tag{3.12}$$

$$Q_m(t) = [I - k_m(t)x_m^H(t)]Q_m(t-1) \tag{3.13}$$

$$t = D, 2D, 3D.....$$

For initialization:

$$Q_m(0) = \beta_m I; \ \beta_m > 0, \tag{3.14}$$

$$\hat{w}_m(0) = 0 \tag{3.15}$$

The superscript $'*'$ denotes complex conjugation and the H indicates Hermitian transposition as usual. σ_n^2 is the variance of measurement noise and I is the unit matrix of dimension $M \times M$. The β_m denotes the degree of uncertainty of m-th subband filter taps, which is taken to be large when initial filter taps are unknown.

NLMS algorithm:

The optimal NLMS algorithm for the m-th subband is obtained as shown in the following:

$$e_m(t) = d_m(t) - \hat{w}_m^H(t-1)x_m(t), \tag{3.16}$$

$$\hat{w}_m(t) = \hat{w}_m(t-1) + \frac{\tilde{\mu}}{\delta + \| x_m(t) \|^2}x_m(t)e_m^*(t), \tag{3.17}$$

where $\tilde{\mu}$ is the adaptation constant given by:

$$0 < \tilde{\mu} < 2\frac{E[| x_m(t) |^2]D(t)}{E[| e_m(t) |^2]},$$

17

$$t = D, 2D, 3D.....$$

$E[| e_m(t) |^2]$ is local error signal power, $E[| x_m(t) |^2]$ is reference m-th subband signal power, and $D(t)$ is mean square deviation. Here $\delta > 0$ and $\hat{w}_m(0) = \mathbf{0}$, as prior knowledge of the tap vector is unknown.

3.1.3 Subband to Wideband Weight Transformation Technique

The wideband filter has N taps, the filter length in each subband is $N/D = 2N/M$, with $D = M/2$. An N/D-point FFT is calculated on the adaptive weights in each subband. These are subsequently stacked to form a $[0...(N/2-1)]$ element of array. The array is then completed by setting element $N/2$ to zero and using the complex conjugate of elements $[1...(N/2-1)]$ in reverse order. Finally, the N element array is transformed by a N-point inverse FFT to obtain the wideband filter weights [30], [39].

A numerical example is presented here to illustrate the subband to wideband mapping. Consider the design, of an AEC with $N = 512$ filter taps and $M = 32$ subband. MATLAB fir1(127,1/32) routine is used for the design of $K = 128$-tap lowpass prototype filter. More sophisticated techniques can be employed in the filter design to achieve overall flat response [18], [33]. Fig. 3.5 shows the
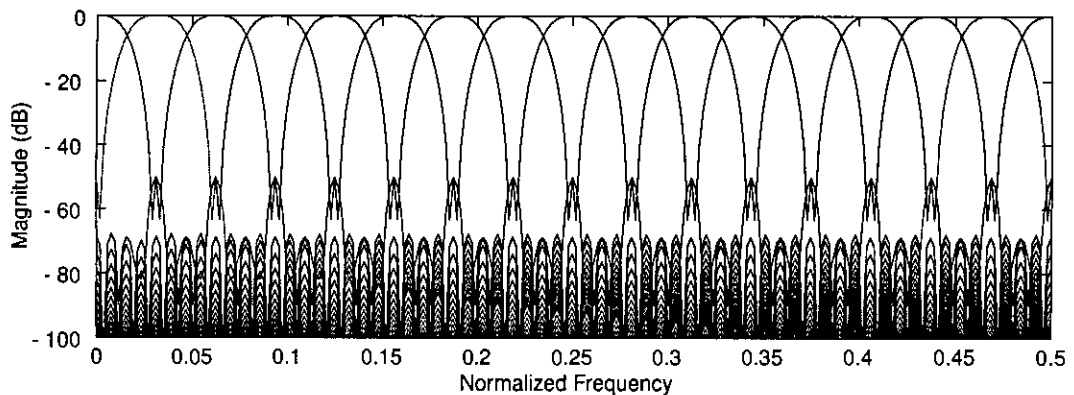
Fig. 3.5: Frequency response of the first $M/2 + 1 = 17$ filters.

resulting frequency response of the first $M/2 + 1 = 17$ filters which are used to extract the complex subband signals. Fig 3.6 clearly depicts how uncorrelated split subbands are piled or stacked in the wideband. Note that, decimation has the effect of stretching the interval. The interval from 0 to π/M now covers the

18
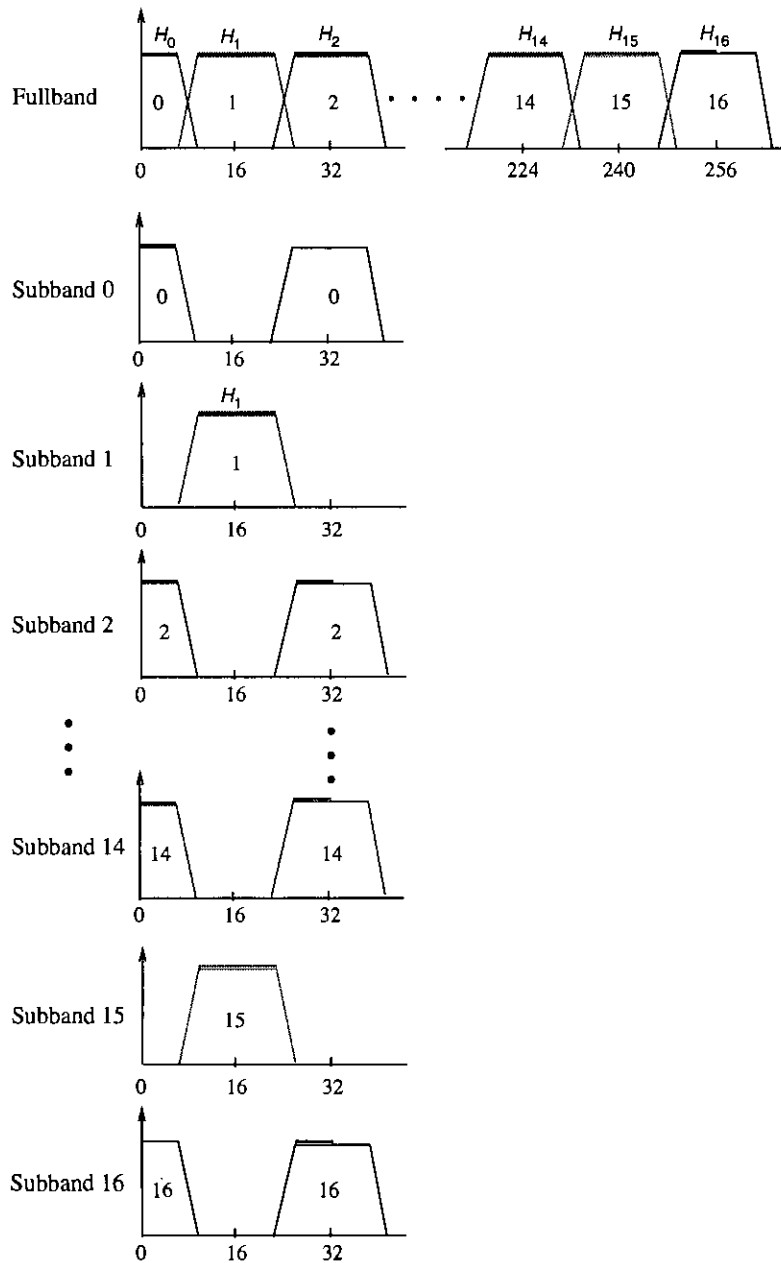
Fig. 3.6: Example of frequency stacking for 32-subband polyphase FFT implementation with 512-point impulse response and 32 taps per subband.

19

band from 0 to π in the the frequency domain. As already stated, even subbands are centered at dc while odd subbands are centered at one half of the decimated sampling frequency [30]. The correspondence between the FFT bins for the subband filter and the full-band filter are given according to Table 3.1. The example given here is only for illustration; the general technique can accommodate an arbitrary number of taps, number of subbands, decimation factor, etc.

Table 3.1: Frequency mapping from subband FFT bin numbers to wideband FFT bin numbers for a 32-subband polyphase FFT implementation with 512-point impulse responses and 32 taps per subband

Subband FFT Bin Number	Wideband FFT Bin Number						
	SB 0	SB 1	SB 2	...	SB 14	SB 16	SB 16
0	0	—	32		224	—	—
1	1	—	33		225	—	—
2	2	—	34		226	—	—
3	3	—	35		227	—	—
4	4	—	36		228	—	—
5	5	—	37		229	—	—
6	6	—	38		230	—	—
7	7	—	39		231	—	—
8	—	8	—		—	232	—
9	—	9	—		—	233	—
10	—	10	—		—	234	—
11	—	11	—		—	235	—
12	—	12	—		—	236	—
13	—	13	—		—	237	—
14	—	14	—		—	238	—
15	—	15	—		—	239	—
16	—	16	—		—	240	—
17	—	17	—		—	241	—
18	—	18	—		—	242	—
19	—	19	—		—	243	—
20	—	20	—		—	244	—
21	—	21	—		—	245	—
22	—	22	—		—	246	—
23	—	23	—		—	247	—
24	—	—	24		216	—	248
25	—	—	25		217	—	249
26	—	—	26		218	—	250
27	—	—	27		219	—	251
28	—	—	28		220	—	252
29	—	—	29		221	—	253
30	—	—	30		222	—	254
31	—	—	31		223	—	255

3.2 Proposed Delayless Subband Acoustic Echo Canceler using Parallel Kalman Filters

The acoustic echo canceler has been implemented using the proposed subband PKF algorithm as shown in Fig. 3.7. To decompose the signals, the same procedure described in Sec. (3.1.1) is followed.
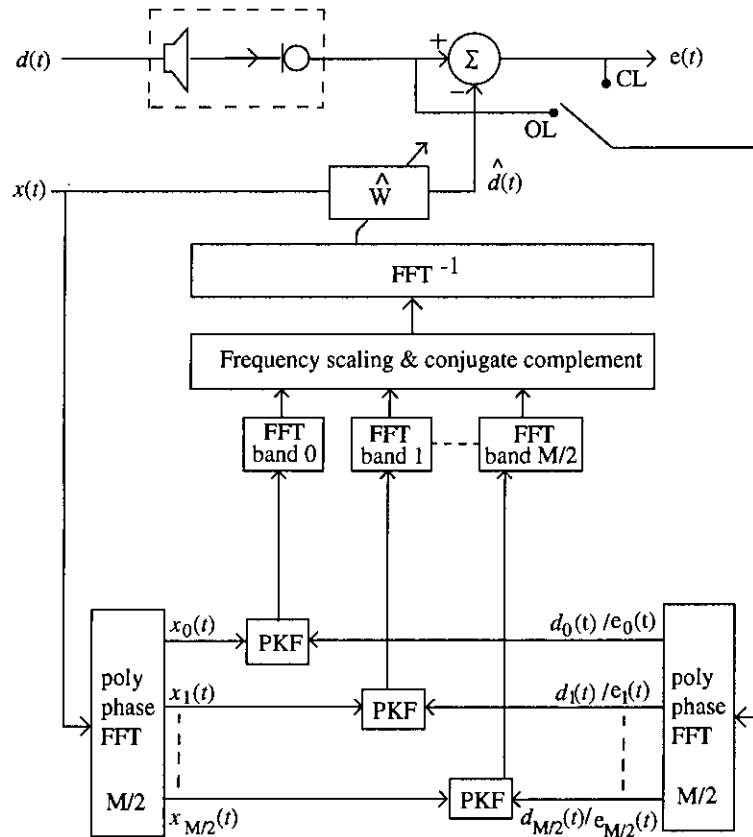
Fig. 3.7: Proposed delayless subband echo canceler using parallel Kalman filters

3.2.1 Configuration of Parallel Kalman Filters in Subband Domain

In this work, adaptive weights are computed in the subband domain using the complex PKF algorithm and then collectively transformed into frequency domain using the FFT, appropriately stacked, and inverse transformed to obtain the wideband filter coefficients, thereby eliminating any delay associated with the cancellation signal. For N wideband adaptive weights and a decimation factor D, there are N/D adaptive weights for each subband. Let w_m is a vector of

22

N/D subband weights, $\boldsymbol{x}_m(t) \equiv [x(t), x(t-D), ..., x(t-N+D)]^T$ is a vector comprising the N/D most recent signals of the subband filter reference signal. Each subband signal is split into J segments for coefficients adaptation using the PKF algorithm as shown in Fig. 3.8 for the m-th subband. The adaptive weights
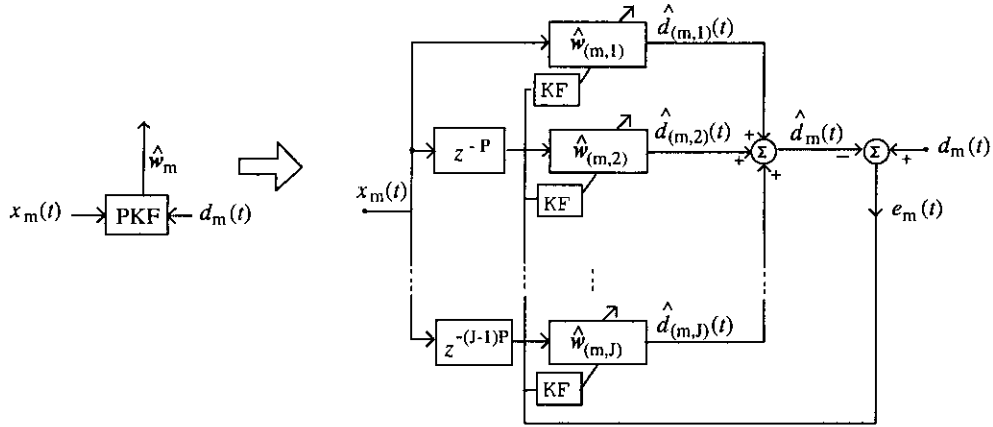
Fig. 3.8: Configuration of the parallel Kalman filters of m-th subband.

of each subband are divided into J parts, namely Part 1, Part 2,..., Part J. As an example, the m-th subband FIR adaptive filter weights $\boldsymbol{w}_m$ in the z-domain can be represented as

$$W_m(z) = \sum_{i=0}^{N/D-1} w_{(m,i)} z^{-i} \tag{3.18}$$

If we divide the adaptive weights of the m-th subband, $\boldsymbol{w}_m$ into J parts, then $\boldsymbol{w}_m$ can be expressed as

$$\begin{aligned} \boldsymbol{w}_m &= \left[w_{(m,0)}, w_{(m,1)}, ..., w_{(m,N/D-1)}\right]^T, \\ &= \left[\boldsymbol{w}_{(m,1)}^T, \boldsymbol{w}_{(m,2)}^T, ..., \boldsymbol{w}_{(m,J)}^T\right]^T \end{aligned} \tag{3.19}$$

The adaptive weights of each part of the m-th subband are given by

$$\boldsymbol{w}_{(m,i)} = \left[w_{(m,P(i-1))}, w_{(m,P(i-1)+1)}, ..., w_{(m,Pi-1)}\right]^T, \tag{3.20}$$

$$i = 1, 2, ..., J$$

where $P = N/(JD)$ is the number of elements of each part and J denotes the number of division in each subband. In Eq. (3.20), $w_{(m,P(i-1))}$ denotes the $P*(i-1)$-th coefficient of the m-th subband. If necessary some zeros should be added to the J-th part of the adaptive weights so as to make $P = N/(JD)$ an integer.

We divide the m-th subband signal $\boldsymbol{x}_m(t)$ into J parts expressed as

$$\boldsymbol{x}_m(t) = [\boldsymbol{x}_{(m,1)}^T(t), \boldsymbol{x}_{(m,2)}^T(t), ..., \boldsymbol{x}_{(m,J)}^T(t)]^T \tag{3.21}$$

Here, $\boldsymbol{x}_{(m,i)}(t)$ represents the m-th subband signals of the i-th part defined as

$$\boldsymbol{x}_{(m,i)}(t) = [x_m(t - P(i-1)D), x_m(t - (P(i-1)D + D)),..$$
$$.., x_m(t - (P(i-1)D + (P-1)D))] \tag{3.22}$$

The J segments of the impulse response described in Eq. (3.20) are estimated using J number of parallel filters. The total output of the J pieces of the filters in parallel is given by

$$\hat{d}_m(t) = \sum_{i=1}^{J} \hat{d}_{(m,i)}(t) = \sum_{i=1}^{J} \hat{\boldsymbol{w}}_{(m,i)}^H(t-1)\boldsymbol{x}_{(m,i)}(t) \tag{3.23}$$

where $\hat{d}_m(t)$ is the estimated subband disturbance signal at time t, and $\hat{\boldsymbol{w}}_{(m,i)}(t)$ denotes the estimated weight vector. Notice that the order of the resultant filter in each subband is JP.

3.2.2 Estimation Algorithm

To obtain the optimal solution of the coefficients of the resultant filter, the local error $e_m(t)$ is used to estimate the parameters.

Proposed PKFs algorithm:

The optimal PKFs algorithm for the i-th part in the m-th subband is obtained as shown in the following:

$$\boldsymbol{k}_{(m,i)}(t) = \frac{\boldsymbol{Q}_{(m,i)}(t-1)\boldsymbol{x}_{(m,i)}(t)}{\sigma_n^2 + \sum_{l=1}^{J} \boldsymbol{x}_{(m,l)}^H(t)\boldsymbol{Q}_{(m,l)}(t-1)\boldsymbol{x}_{(m,l)}(t)}, \tag{3.24}$$

$$e_m(t) = d_m(t) - \sum_{i=1}^{J} \hat{\boldsymbol{w}}_{(m,i)}^H(t-1)\boldsymbol{x}_{(m,i)}(t), \tag{3.25}$$

$$\hat{\boldsymbol{w}}_{(m,i)}(t) = \hat{\boldsymbol{w}}_{(m,i)}(t-1) + \boldsymbol{k}_{(m,i)}(t)e_m^*(t) \tag{3.26}$$

$$\boldsymbol{Q}_{(m,i)}(t) = [\boldsymbol{I} - \boldsymbol{k}_{(m,i)}(t)\boldsymbol{x}_{(m,i)}^H(t)]\boldsymbol{Q}_{(m,i)}(t-1) \tag{3.27}$$

$$i = 1, 2, ..., J; \quad t = D, 2D, 3D.....$$

For initialization:

$$\boldsymbol{Q}_{(m,i)}(0) = \beta_{(m,i)}\boldsymbol{I}; \ \beta_{(m,i)} > 0, \tag{3.28}$$

$$\hat{\boldsymbol{w}}_{(m,i)}(0) = \boldsymbol{0} \tag{3.29}$$

24

The superscript $'*'$ denotes complex conjugation and the H indicates Hermitian transposition as usual. σ_n^2 is the variance of measurement noise and $\boldsymbol{I}$ is the unit matrix of dimension $P \times P$. The $\beta_{(m,i)}$ denotes the degree of uncertainty of the i-part filter taps of m-th subband, which is taken to be large when initial filter taps are unknown.

PNLMS algorithm:

For the purpose of comparison, PNLMS algorithm is also presented. The optimal PNLMS algorithm for the m-th subband is obtained as shown in the following:

$$e_m(t) = d_m(t) - \sum_{i=1}^{J} \hat{\boldsymbol{w}}_{(m,i)}^H(t-1)\boldsymbol{x}_{(m,i)}(t), \tag{3.30}$$

$$\hat{\boldsymbol{w}}_{(m,i)}(t) = \hat{\boldsymbol{w}}_{(m,i)}(t-1) + \frac{\tilde{\mu}}{\delta + \| \boldsymbol{x}_m(t) \|^2}\boldsymbol{x}_{(m,i)}(t)e_m^*(t), \tag{3.31}$$

where $\tilde{\mu}$ is the adaptation constant given by:

$$0 < \tilde{\mu} < 2\frac{E[| x_m(t) |^2]D(t)}{E[| e_m(t) |^2]},$$

$$i = 1, 2, ..., J; \quad t = D, 2D, 3D.....$$

$E[| e_m(t) |^2]$ is local error signal power, $E[| x_m(t) |^2]$ is reference m-th subband signal power, and $D(t)$ is mean square deviation. Here $\delta > 0$ and $\hat{\boldsymbol{w}}_{(m,i)}(0) = \boldsymbol{0}$, as prior knowledge of the tap vector is unknown. Note that in Eq. (3.31), adaptive constant is normalized using $\| \boldsymbol{x}_m(t) \|^2$ instead of $\| \boldsymbol{x}_{(m,i)}(t) \|^2$ for achieving better convergence rate like the PNLMS algorithm for time domain[4].

For subbband to wideband mapping, estimated weights are stacked as:

$$\hat{\boldsymbol{w}}_m = [\hat{\boldsymbol{w}}_{(m,1)}; \hat{\boldsymbol{w}}_{(m,2)}, ..., \hat{\boldsymbol{w}}_{(m,J)}]; \tag{3.32}$$

Then an N/D-point FFT is calculated on the adaptive weights in each subband, which are then properly stacked as the same procedure described in Sec. (3.1.3).

3.3 Computational Complexity

Here, computational complexity is calculated based on the number of multipliers per input samples, assuming that the product of complex values is implemented.

---

[4]Because of this modification, adaptive filter using PNLMS algorithm in the subband structure performs exactly same to the adaptive filter using NLMS algorithm in the subband structure.

through 4 real multiplies. The overall computational complexity is divided into four parts.

1. *Subband decomposition of $x(t)$ and $d(t)$*: For M subbands, the 2× oversampled subband decomposition [32] requires one convolution of a K-length prototype filter and one M-point real FFT for each block of $M/2$ input samples. Therefore, the subband decomposition requires

$$C_1 = 2K/M + 2\log_2 M \qquad (3.33)$$

real multiplies per input sample.

2. *Updating the adaptive weights*: Since only half of the M complex subband signals are processed and subband filters are downsampled by a factor $D = M/2$, each of the $M/2$ lower subbands has to update $2N/M$ complex adaptive weights for each block of $M/2$ input samples. For close-loop version, with NLMS or PNLMS algorithm this requires

$$C_2^{NLMS/PNLMS} = 8N/(p_s * M) \qquad (3.34)$$

real multiplies per input sample. Here p_s denotes the number of parallel section in each subband. For KF or PKF, the value of C_2 is given by

$$C_2^{PKFs} = 8(2N/(p_s * M))^2 + 16(2N/(p_s * M)) \qquad (3.35)$$

For open-loop version, an additional C_2 real multiplies per input sample are required to evaluate the subband signal path convolutions [13].

3. *Subband to Wideband mapping*: The subband-to-wideband filters mapping requires a $2N/M$-point complex FFT for each of the $M/2$ lower subbands and an N-point inverse real FFT. An $2N/M$-point complex FFT requires about $4N/M\log_2(2N/M)$ real multiplies. In practice, the wideband weights transformations are performed every N/J input samples, because the wideband filter output cannot change much faster than the length of its impulse response [30]. Typical value of J is in the range one to eight. This part thus requires

$$C_3 = [2\log_2(2N/M) + \log_2 N]J \qquad (3.36)$$

26

real multiplies per input sample.

4. *Wideband signal path convolution:* The wideband convolution is performed by partitioning the wideband filter into p segments. The number of multiplies per input sample is given by

$$\begin{aligned}
C_4 &= N_p + 2p \log_2(2N_p) + 4(p-1) + 2\log_2(2N_p) \\
&= N/p + 2(p+1)\log_2(2N/p) + 4(p-1)
\end{aligned} \tag{3.37}$$

considering that the product of complex values is implemented through 4 real multiplies. Here $N_p = N/p$ and the value of p is optimized so that the complexity over the direct convolution is optimized. Thus the total number of real multiplications required for the open-loop echo canceler is

$$C_{OL} = C_1 + 2C_2 + C_3 + C_4 \tag{3.38}$$

for the close-loop echo canceler is

$$C_{CL} = C_1 + C_2 + C_3 + C_4 \tag{3.39}$$

As a comparison, it is to be noted that the computational complexity of the fullband LMS algorithm is approximately $2N$ and that of fullband Kalman filter is $8N^2 + 16N$ [16].

Chapter 4

Simulation Results

Simulation results are presented comparing the performance of different adaptation algorithms used in AECs. The chapter concludes with some remarks.

4.1 Parameters used to Asses an AEC

To evaluate the modified AEC, we present several computer simulation results. The AEC performance is assessed by using three objective measured. The first one is the steady state echo return loss enhancement (ERLE), expressed as

$$\text{ERLE}(t) \equiv 10 \log_{10} \frac{\text{average power of } \hat{d}(t)}{\text{average power of } e(t)} \qquad (4.1)$$

where $t - S \leq j \leq t$, S is the number of samples taken to calculate steady state ERLE. Thus, ERLE is the additional reduction in echo level accomplished by the echo canceler. An echo canceler is not a perfect device; the best it can do is attenuate the level of the returning echo. ERLE is a measure of this echo attenuation performed by the echo canceler. The second objective measure is the time of initial convergence (TIC) to a specified level of ERLE. The third objective measure is the number of multiplies required for computation.

4.2 Different Models used in Simulation

Two different reference signals $(x(t))$ are considered. The color stationary signal is obtained from the output of the ARMA model of Eq. (4.2)

$$
\begin{aligned}
x(t) &= 0.4x(t-1) - 0.34x(t-2) + 0.396x(t-3) - 0.7565x(t-4) + u(t) \\
&\quad - 0.1u(t-1) - 1.37u(t-2) + 0.353u(t-3) + 0.6984u(t-4), \qquad (4.2)
\end{aligned}
$$

where $u(t)$ is zero-mean white noise [16]. See Fig. 4.1. The speech signal "Hello" is used as the nonstationary input signal. This signal is depicted in Fig. 4.2. Three different echo paths are considered. The assumed length of them are 512, 1024 and 2048. See Fig. 4.3-4.5. The value of S to calculate the steady state ERLE is taken to be 200, 400 and 600. The echo-ed signal or the micsignal $d(t)$ is obtained from these echo paths for simulation purpose. To decompose the signals into 8, 16, 32, and 64 subbands, we use the MATLAB fir1(31,1/8), fir1(63,1/16), fir1(127,1/32), fir1(255,1/64) routine, respectively. As the polyphase FFT implementation is assumed, only $M/2 + 1$ subband signals are estimated in all cases. Only open-loop configuration is considered.
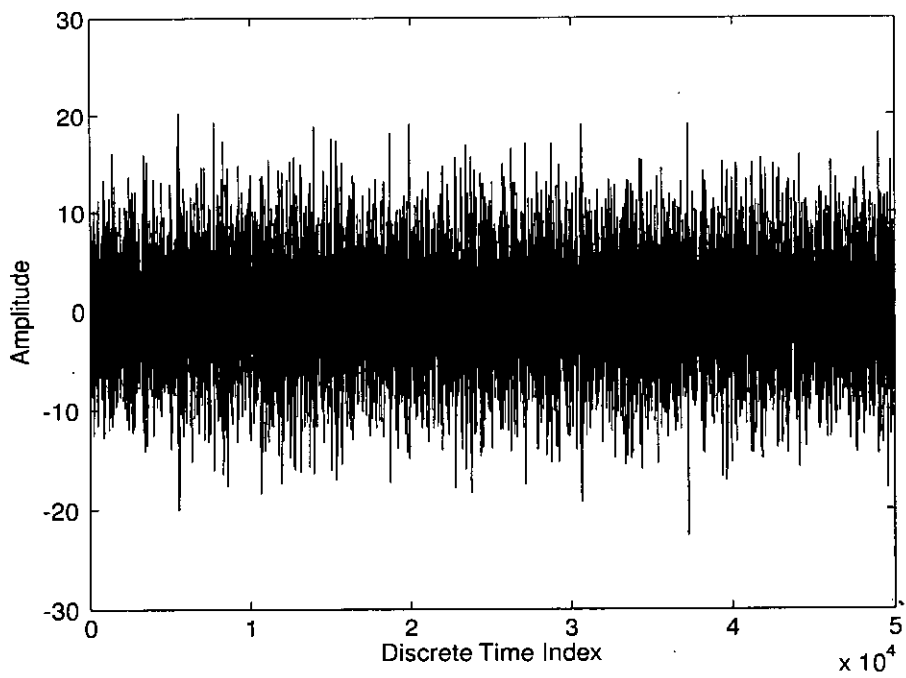
Fig. 4.1: Color signal used as stationary reference signal.
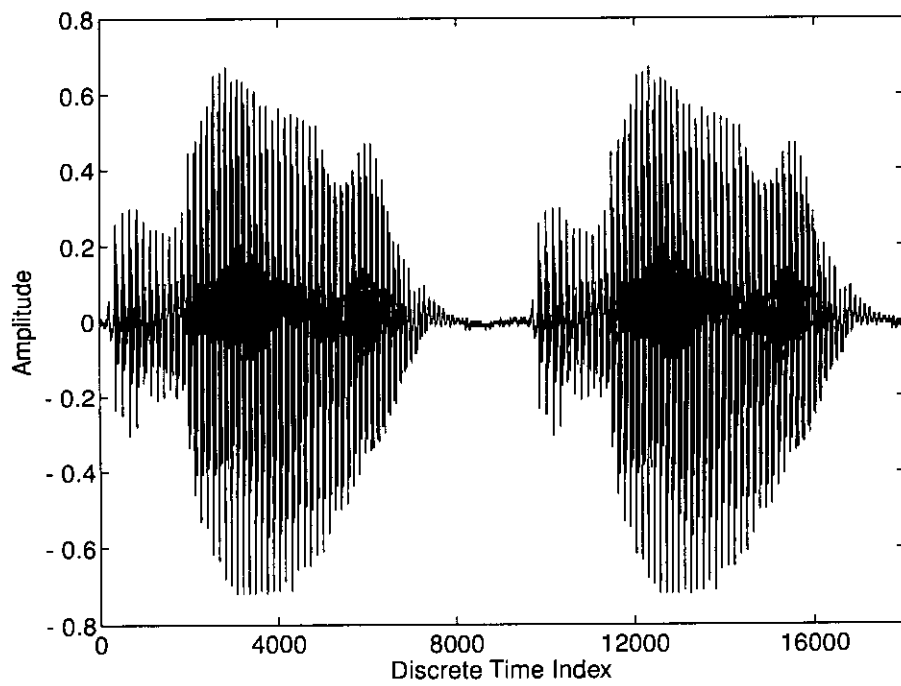

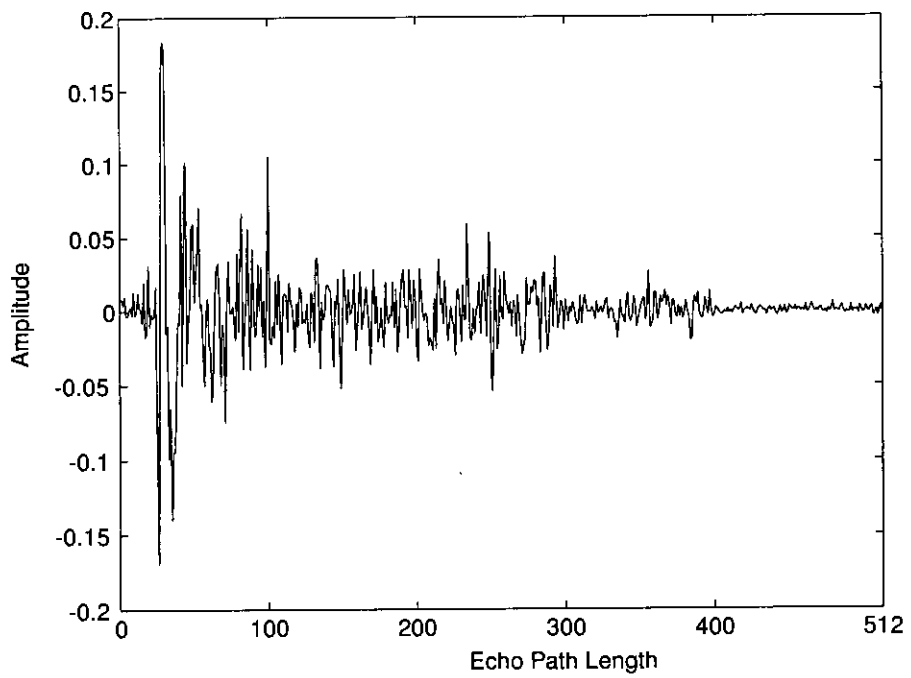Fig. 4.2: Reference signal "Hello".

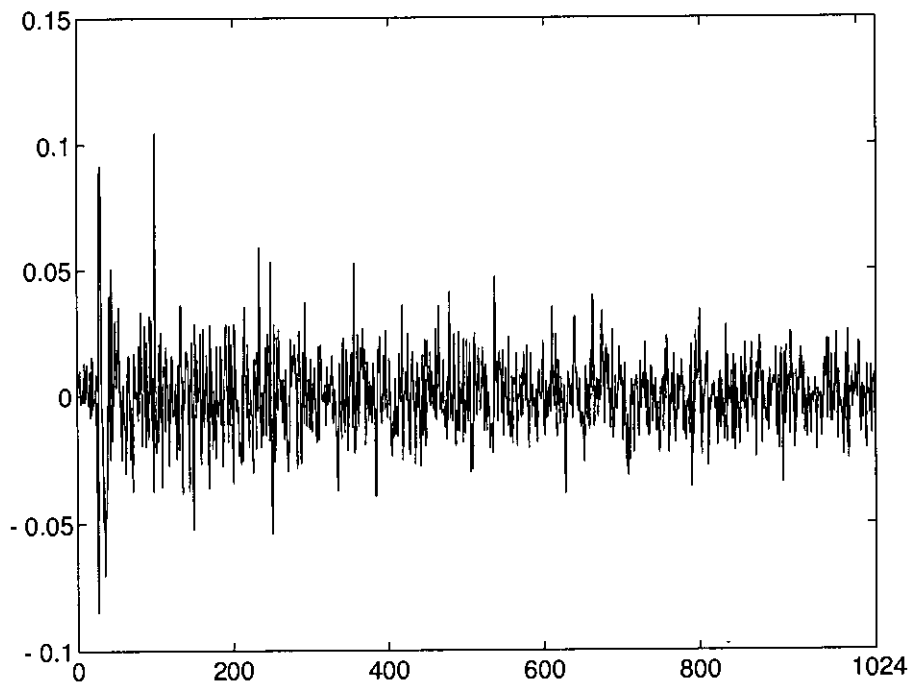Fig. 4.3: Impulse response of echo path 1 of length 512.

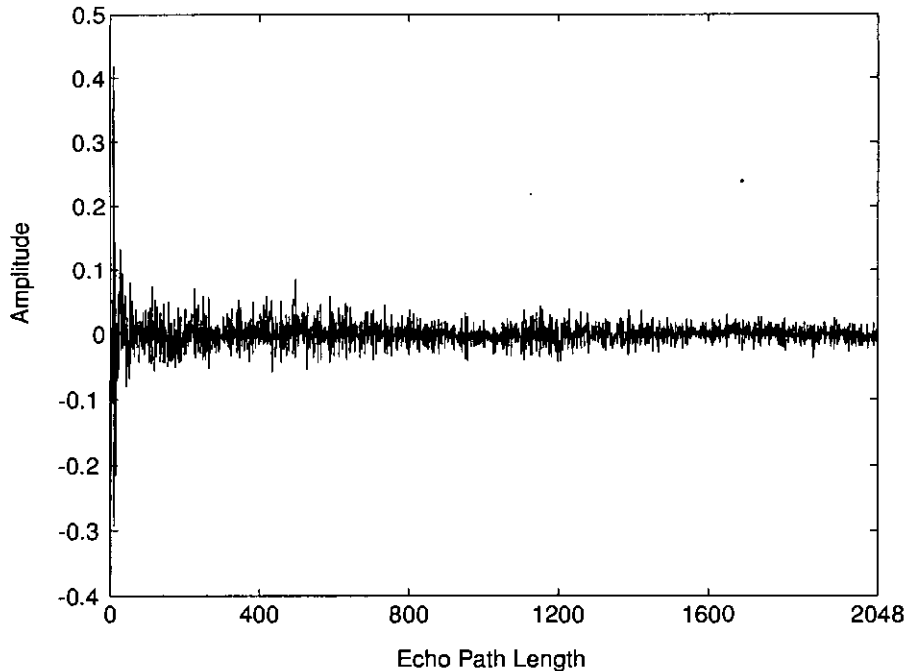Fig. 4.4: Impulse response of echo path 2 of length 1024.

31

Fig. 4.5: Impulse response of echo path 3 of length 2048.

4.3 Results and Comparisons

1. *Echopath of length 512:* For comparison among different algorithms, consider
the design of an $N = 512$ tap real wideband AEC. The performance is evalu-
ated using two reference signals (color and speech). Fig. 4.6 and 4.7 show
ERLE obtained for different algorithms namely PNLMS, KF and PKFs for color
and speech signal, respectively. As expected, with equal number of subbands,
KF/PKFs show better results than the conventional NLMS/PNLMS filter. The
number of real multiplications required and ERLE obtained after 4000 iterations
for each adaptive scheme are calculated and summarized in Table 4.1. The com-
putational complexity is very large for KF than that of NLMS/PNLMS. But
computational complexity drastically reduces for PKF's. As for example, with
$M = 16$ and $p_s = 1$, the number of real multiplies required for NLMS is 511
and that for KF is 4863. Whereas, with $M = 16$ and $p_s = 8$, the number of
real multiplies required for PKFs is only 383. For color signal, with $M = 16$ and
$p_s = 8$, ERLE obtained for PNLMS is 17.52 and that for PKFs is 30.67. Also,
for speech signal, with $M = 16$ and $p_s = 8$, ERLE obtained for PNLMS is 8.28
and that for PKFs is 20.46. Hence the proposed AEC, which utilizes PKFs in
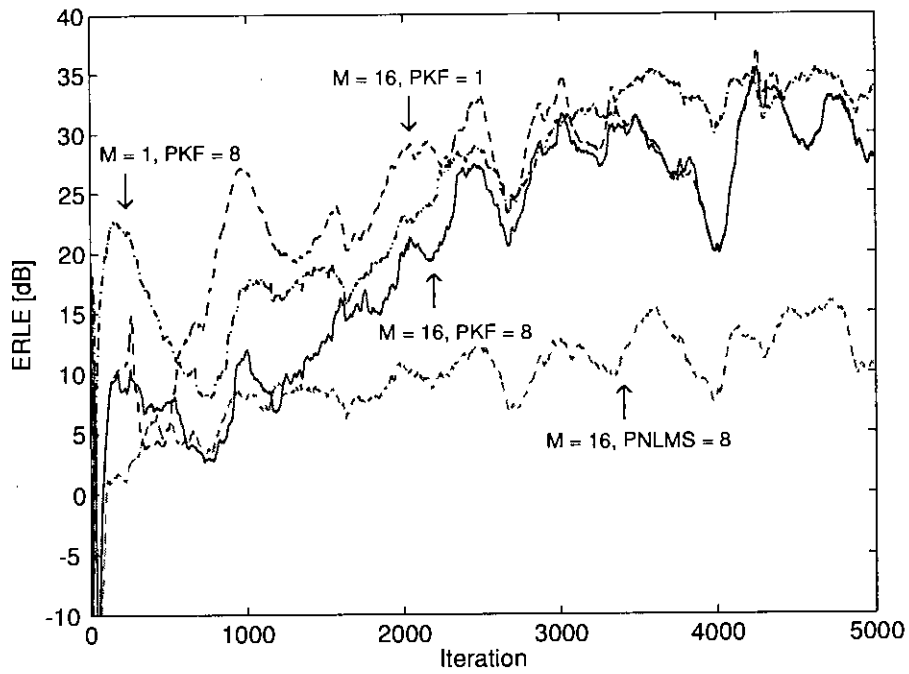the subband structure for coefficients adaptation, has a significant performance

Fig. 4.6: ERLE obtained by different algorithms of the AEC of length 512 with color signal as a reference signal.
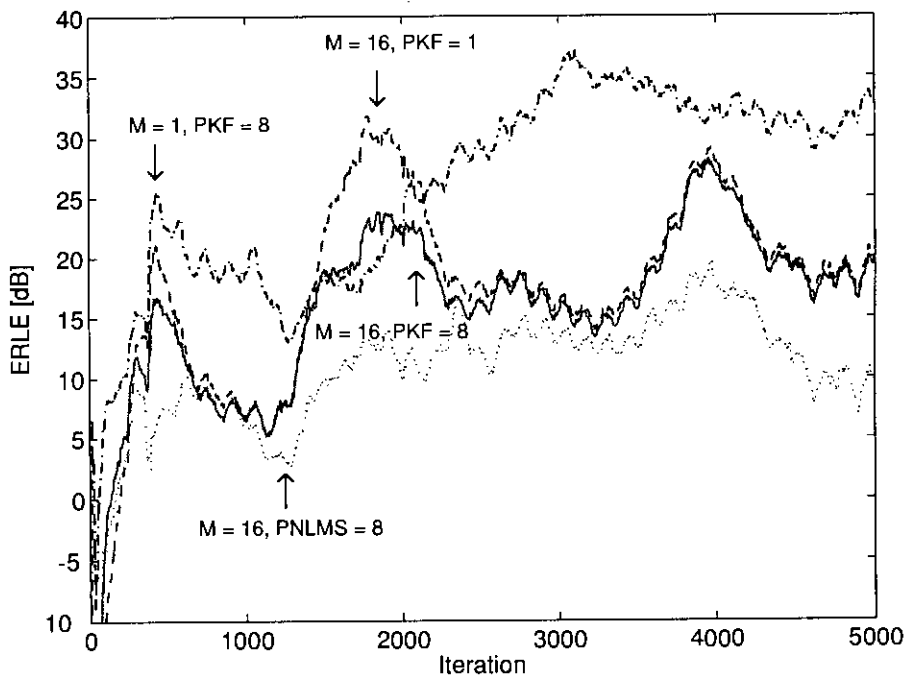

Fig. 4.7: ERLE obtained by different algorithms of the AEC of length 512 with speech signal as a reference signal.

Table 4.1: Comparison of computational complexity and ERLE for echo path 1 of length 512.

Type of reference signal	No. of subbands (M)	No. of parallel sections per subband	LMS algorithm		Kalman algorithm	
			C	ERLE	C	ERLE
Color	16	1	511	17.52	4863	27.88
	16	4	319	17.52	639	27.59
	16	8	287	17.52	383	30.67
	1	8	-	-	133338	30.78
Speech	16	1	511	8.28	4863	20.35
	16	4	319	8.28	639	20.33
	16	8	287	8.28	383	20.46
	1	8	-	-	133338	32.28

advantage over the traditional DSAEC in terms of the convergence rate and computational efficiency.

2. *Echopath of length 1024:* Now, consider the design of an $N = 1024$ tap real wideband AEC. The performance is evaluated using two reference signals (color and speech) as usual. Fig. 4.8 and 4.9 show ERLE obtained for different algorithms namely PNLMS, KF and PKFs for color and speech signal, respectively. The number of real multiplications required and ERLE obtained after 5000 iterations for each adaptive scheme are calculated and summarized in Table 4.2. As expected, with equal number of subbands, KF/PKFs show better results than the conventional NLMS/PNLMS filter. The computational complexity is very large for KF than that of NLMS/PNLMS. But computational complexity drastically reduces for PKFs. As for example, with $M = 32$ and $p_s = 1$, the number of real multiplies required for NLMS is 852 and that for KF is 17748. Whereas, with $M = 32$ and $p_s = 8$, the number of real multiplies required for PKFs is only 724. For color signal, with $M = 32$ and $p_s = 8$, ERLE obtained for PNLMS is 11.03 and that for PKFs is 21.84. Also, speech signal, with $M = 32$ and $p_s = 8$, ERLE obtained for PNLMS is 11.67 and that for PKFs is 19.83. Although PKFs in the time domain show better convergence rate, they require a huge amount of computational complexity. So, for both types of reference signal, the proposed AEC show better results in terms of both ERLE and computational complexity.
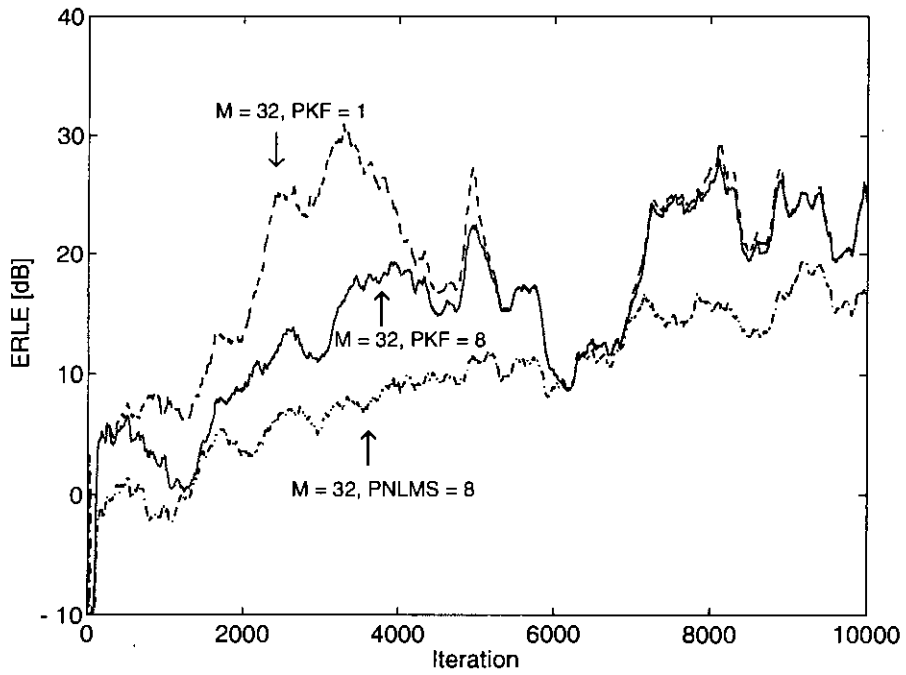
Fig. 4.8: ERLE obtained by different algorithms of the AEC of length 1024 with color signal as a reference signal.
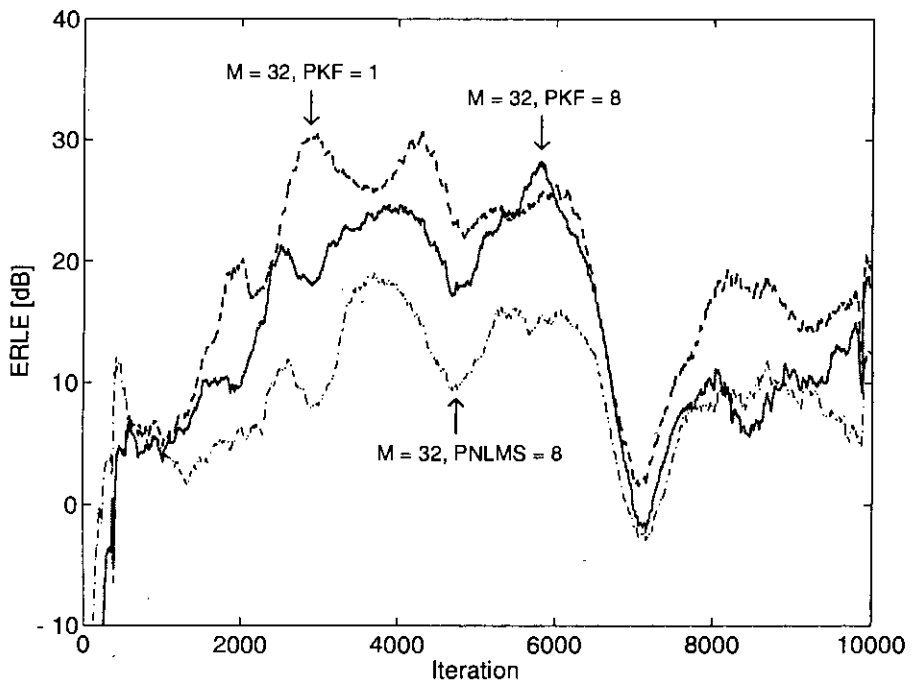

Fig. 4.9: ERLE obtained by different algorithms of the AEC of length 1024 with speech signal as a reference signal.

35

Table 4.2: Comparison of computational complexity and ERLE for echo path 2 of length 1024.

Type of reference signal	No. of subbands (M)	No. of parallel sections per subband	LMS algorithm		Kalman algorithm	
			C	ERLE	C	ERLE
Color	32	1	852	11.03	17748	24.83
	32	4	468	11.03	1620	22.45
	32	8	404	11.03	724	21.84
	1	16	-	-	133420	-
Speech	32	1	852	11.67	4863	23.47
	32	4	468	11.67	1620	21.54
	32	8	404	11.67	724	19.83
	1	16	-	-	133420	-

3. *Echopath of length 2048:* The assumed length (N) of the acoustic "echo path 3" is 2048. As usual, the performance of the AEC is evaluated by two reference signals (color and speech). Fig. 4.10 and 4.11 show ERLE obtained for different algorithms namely PNLMS, KF and PKFs for color and speech signal respectively. As expected, with equal number of subbands, KF/PKFs show better results than the conventional NLMS/PNLMS filter. The number of real multiplications required and ERLE obtained after 12000 iterations for each adaptive scheme are calculated and summarized in Table 4.3. The computational

Table 4.3: Comparison of computational complexity and ERLE for echo path 3 of length 2048.

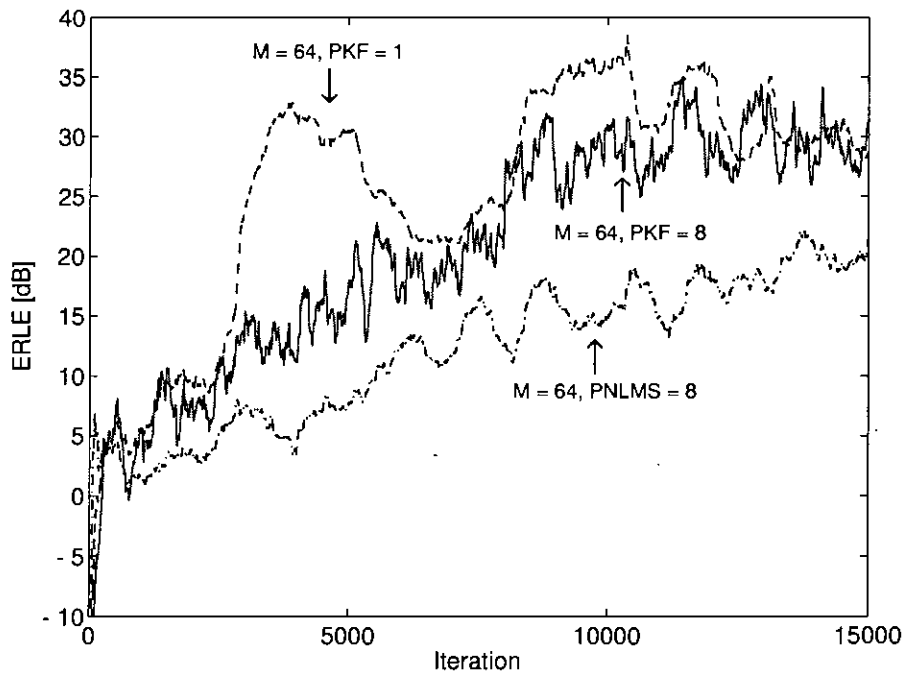| Type of reference signal	No. of subbands (M)	No. of parallel sections per subband	LMS algorithm		Kalman algorithm	
			C	ERLE	C	ERLE
Color	64	1	1001	17.87	17897	35.29
	64	4	617	17.87	1769	33.00
	64	8	553	17.87	873	28.52
	1	32	-	-	133566	-
Speech	64	1	1001	14.07	17897	18.73
	64	4	617	14.07	1769	10.69
	64	8	553	14.07	873	22.57
	1	32	-	-	133566	-

Fig. 4.10: ERLE obtained by different algorithms of the AEC of length 2048 with color signal as a reference signal.
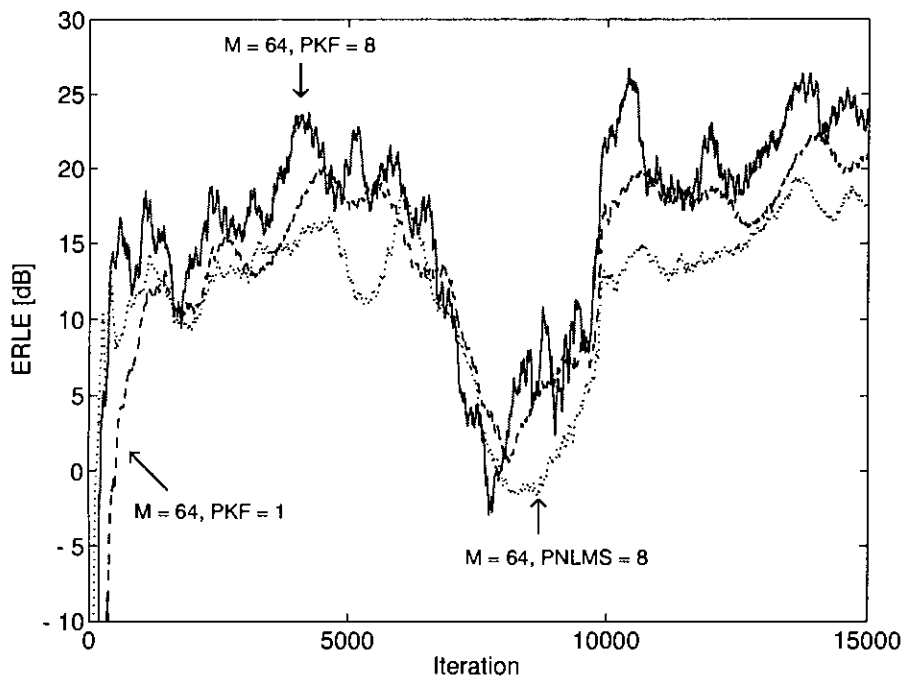

Fig. 4.11: ERLE obtained by different algorithms of the AEC of length 2048 with speech signal as a reference signal.

complexity is very large for KF than that of NLMS/PNLMS. But computational complexity drastically reduces for PKFs. As for example, with $M = 64$ and $p_s = 1$, the number of real multiplies required for NLMS is 1001 and that for KF are 17897. Whereas, with $M = 64$ and $p_s = 8$, the number of real multiplies required for PKFs is only 873. Note that for time domain PKFs, we don't even dare to evaluate its performance due to high computational complexity. For color signal, with $M = 64$ and $p_s = 8$, ERLE obtained for PNLMS is 17.87 and that for PKFs is 28.52. Also, speech signal, with $M = 64$ and $p_s = 8$, ERLE obtained for PNLMS is 14.07 and that for PKFs is 22.57.

Thus it is clear that PKFs show better results in terms of both ERLE and computational complexity when optimal number of parallel sections are incorporated in each subband. Moreover, the computational complexity of PKFs is comparable with that of PNLMS with much better ERLE index.

Chapter 5

Conclusions

In this work, we have designed an echo canceler using optimal number of parallel sections in each subband for coefficient adaptations. Incorporation of parallel architecture in each subband has provided a flexibility in trade-off between the number of subbands and parallel filters in each subband for optimum performance of subband adaptive filters. Like the conventional DSAEC, it hasn't suffered from the inherent delay usually found in subband schemes. On the other hand, by employing PKFs in the subband domain, it has yielded improved convergence rate over the conventional DSAEC. The computational complexity has founded to be very large for KF even in the subband domain than that of NLMS and PNLMS. But computational complexity has drastically reduced for PKFs. Moreover, the computational complexity of PKFs has became comparable with that of PNLMS with much better ERLE index. Hence the proposed AEC, which utilizes PKFs in the subband structure for coefficients adaptation, has a significant performance improvement over the traditional DSAEC in terms of both the convergence rate and computational efficiency when optimal number of parallel sections are incorporated in each subband.

5.1 Future Plan

A number of additional studies would be interesting to perform on our proposed AEC. The performance of the PKFs has degraded somewhat with the increase of parallel sections in the subband domain. PKFs algorithm should be modified so as to make its performance similar to that of KF. In this work we didn't consider the noise affect. Over the past few decades there has been a tremendous increase

in the level of ambient environmental noise. A new echo cancellation method based on the combined acoustic echo cancellation and noise reduction structure can be proposed. In this study the simulations were run off-line. The system should be implemented running in real-time to evaluate the performance of the AEC under more realistic circumstances.

Bibliography

[1] S. Haykin, *Adaptive filter theory.*, Pearson Education (Singapore) Pte. Ltd., 2002.

[2] S. K. Mitra, *Digital signal processing: a computer-based approach.*, Tata McGraw-Hill, 2001.

[3] J. Huo, S. Nordholm, and Z. Zang, "A new subband to fullband transformation for delayless subband adaptive filtering," IFCC'00 (Bankok), 2000.

[4] R. Abouchakra, "Delay Estimation or Transform Domain Acoustical Echo Cancellation," Master of Enginnering dessertation, Univ. McGill, Canada, Sep. 1997.

[5] T. Petillon, A. Gilloire, and S. Theodoridis, "The fast Newton transversal filter: An efficient scheme for acoustic echo cancellation in mobile radio," *IEEE Trans. Signal Processing,* vol. 42, pp. 509-518, Mar. 1994.

[6] J. L. Kelly and R. F. Logan, *Self-adaptive echo canceller.*, U.S. Patent 3,500,000, Mar. 10, 1970.

[7] M. M. Sondhi, "An adaptive echo canceler," *Bell Syst. Tech. J.,* 46:497-510, Mar. 1967.

[8] M. M. Sondhi, *Echo canceller.*, U.S. Patent 3,499,999, Mar. 1970.

[9] P. Diniz, *Adaptive Filtering: Algorithms and Practical Implementation.*, Boston, MA: Kluwer Academic, 1997.

[10] B. Widrow and S. D. Steams, *Adaptive Signal Processing.*, Prentice-Hall, Englewood Cliffs, NJ, 1985.

[11] G. A. Clark, S. K. Mitra, and S. R. Parker, "Block implementation of adaptive digital filters," *IEEE Trans. Circuits Syst.*, vol. CAS-28, pp. 584-592, 1981.

[12] K. P. J. Soo, "Multidelay block frequency domain adaptive filters," *IEEE Trans. Acoust., Speech, Signal Processing,* vol. 38, no.2, pp. 373-376, 1990.

[13] P. J. VanGerwen, F. A. M. van de Laar and J. J. Kotmans, "Digital echo canceler," U.S. Patent 4,903,247, 1990.

[14] J. M. Cioffi and J. A. C. Bingham, "A data-driven multitone echo canceler," *Proc. IEEE GLOBECOM '91*, pp. 2.4.1-2.4.5, 1991.

[15] Merched and A. H. Sayed, "An embedding approach to frequency-domain and subband adaptive filtering," *IEEE Trans. Signal Processing*, vol. 48, no. 9, pp. 2607-2619, 2000.

[16] J. Cao, T. Yahagi and J. Lu, "Parallel adaptive infinite impulse response digital filters using Kalman filters," *Electronics and Communications in Japan*, Part 3, vol. 78, no. 2, 1995.

[17] J. J. Shynk, "Frequency-domain and multirate signal processing," *IEEE Signal Processing Mag.*, vol. 9, pp. 14-37, 1992.

[18] P. P. Vaidyanathan, *Multirate Systems and Filter Banks.*, Englewood Cliffs, NJ: Prentice-Hall 1993.

[19] N. J. Fliege, *Multirate Digital Signal Processing.*, New York: Wiley, 1994.

[20] M. Schönle, N. J. Fliege, and U. Zölzer, "Parametric approximation of room impulse response by multirate systems," in *Proc. IEEE ICASSP-93,* vol. 1, pp. 153-156, 1993.

[21] A. Gilloire and M. Vetterli, "Adaptive filtering in subbands with critical sampling: Analysis, experiments, and application to acoustic echo cancellation," *IEEE Trans. Signal Processing*, vol. 40, no. 8, 1862-1875, 1992.

[22] J. E. Hart, P. A. Naylor, and O. Tanrikulu, "Polyphase all-pass IIR structures for sub-band acoustic echo cancellation," in *Proc. EUROSPEECH-93,* Berlin, Germany, Sept. 1993, pp. 1813-1816.

[23] M. Courville and P. Duhamel, "Adaptive filtering in sub-bands using a weighted criterion," in *Proc. ICASSP-95,* Detroit, MI, pp. 985-988, May 1995.

[24] W. Kellermann, "Analysis and design of multirate systems for cancellation of acoustical echoes," in *ICASSP-88,* NY, Apr. 1988, pp. 2570-2573.

[25] S. S. Pradhan and V. U. Reddy, "A New Approach to Subband Adaptive Filtering," *IEEE Trans. on signal Processing,* vol. 47, no. 3, pp. 655-664, Mar. 1999.

[26] S. Weiss and R. W. Stewart "On the optimality of subband adaptive filters," in *Proc. IEEE Workshop on Applications of Signal Processing to Audio and Acoustics,* New Paltz, New York, pp. W99-1-W99-4, Oct. 1999.

[27] D. T. M. Slock, "Fractionally-spaced subband and multiresolution adaptive filters," in *ICASSP-91,* Toronto, Ont., Canada, pp. 3693-3696, May 1991.

[28] R. W. Stewart "Design of Near Perfect Reconstruction Oversampled Filter Banks for Subband Adaptive Filters," *IEEE Trans. on Circuit and System-II: Analog and Digital Signal Processing,* vol. 46, no. 8, pp. 1081-1085, Aug. 1999.

[29] P. A. Naylor and J. E. Hart, "Subband acoustic echo control using noncritical frequency sampling," in *Proc. EUSIPCO-96,* Trieste, Italy, Sept. 1996, pp. 37-40.

[30] D. R. Morgan, J. C. Thi, "A delayless subband adaptive filter architecture," *IEEE Trans. Signal Processing.,* vol. 43, no. 8, pp. 1819-1830, 1995.

[31] F. Wallin, "Combining acoustic echo cancellation and suppression," Master's thesis, Linköping Univ., Sweden, 2003.

[32] E. R. Ferrara Jr., "Frequency-domain adaptive filtering" in *Adaptive filters,* C. F. N. Cowan and P. M. Grant, Eds. Englewood Cliffs, NJ: Prentice Hall, 1985, chap 6, pp. 145-179.

[33] G. Wackersreuther, "Some new aspects of filter banks," *IEEE Trans. Acoust., Speech, Signal Processing.,* vol. ASSP-34, pp. 1182-1200, 1986.

[34] S. J. Park, C. Lee, and D. H. Youn, "A residual echo cancelletion scheme for hands-free telephony," *IEEE Signal Processing Lett.*, vol. 9, no. 12, pp. 397-399, Dec. 2002.

[35] J. Benesty, D. R. Morgan, and J. H. Cho, "A new class of double talk derectors based on cross correlations," *IEEE Trans. Speech Auodio Processing,* vol. 8, pp. 168-172, Mar. 2000.

[36] S.C. Douglas, T.H.Y. Meng, "Normalized data nonlinearities for LMS adaptation," *IEEE Trans. Acoust. Speech Signal Processing,* vol. 42, pp. 1352-1365, 1994.

[37] A. Gilloire, "Recent advances in adaptive filtering algorithms for acoustic echo cancellation," in *Proc. Int. Workshop Acoust. Echo Noise Control,* Roros, Norway, pp. 115-134, June 1995.

[38] A. N. Akansu, R. A. Haddad, *Multiresolution signal deomposion.* Academic Press, Inc., San Diego, 1992.

[39] S. Nordholm, J. Nordberg, "Delayless Subband Echo Cancellation," in *Proc. ICSV 5, Fifth International Congress on Sound and Vibration,* Adelaide, Australia, Dec. 1997.

Appendix A

Digital Filter Banks

Uniform filter bank and its polyphase implementation play an important role in deriving complex subband signals and are subject to discussion in this section.

A.1   Uniform Filter Banks

The digital filter bank is a set of digital bandpass filters with either common input or a summed output [2]. There are two types of filter banks, *analysis filter bank* and *synthesis filter bank*. An analysis filter bank consists of a set of filters, with system function $H_m(z)$, arranged in parallel as shown in Fig. A.1(a). A synthesis filter bank consists of a set of filters with system function $F_m(z)$, arranged as indicated in Fig. A.1(b).

Here, a simple technique for the design of the *uniform filter bank*, i.e., filter bank with equal passband widths, has been developed. A casual lowpass digital filter, $H_0(z)$, with passband edge ω_p and stopband edge ω_s around π/M, is defined

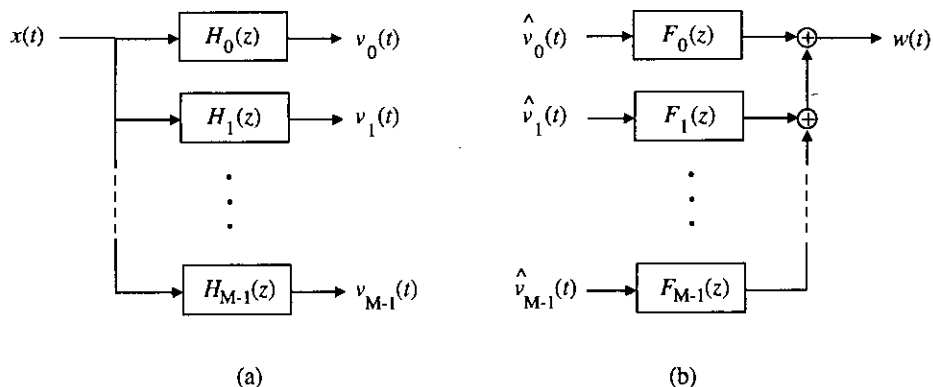
(a)   (b)

Fig. A.1: (a) Analysis filter bank, and (b) Synthesis filter bank.

as

$$H_0(z) = \sum_{k=0}^{\infty} h_0(k)z^{-k} \qquad \text{(A.1)}$$

where $h_0(k)$ is the impulse response of a prototype filter and M is an arbitrary integer. Now, consider the transfer function $H_m(z)$ which can be expressed in the time domain as

$$h_m(k) = h_0(k)e^{\frac{j2\pi mk}{M}}, \qquad m = 0, 1, ..., M-1, \qquad \text{(A.2)}$$

i.e.,

$$h_m(k) = h_0(k)W_M^{-mk}, \qquad m = 0, 1, ..., M-1, \qquad \text{(A.3)}$$

where $W_M = ^{-j2\pi/M}$. Thus,

$$H_m(z) = \sum_{k=0}^{\infty} h_m(k)z^{-k} = \sum_{k=0}^{\infty} h_0(k)(zW_M^m)^{-k}, \qquad m = 0, 1, ..., M-1, \qquad \text{(A.4)}$$

or,

$$H_m(z) = H_0(zW_M^m) \qquad m = 0, 1, ..., M-1, \qquad \text{(A.5)}$$

with a corresponding frequency response

$$H_m(e^{j\omega}) = H_0(e^{j(\omega-2\pi m/M)}), \qquad m = 0, 1, ..., M-1 \qquad \text{(A.6)}$$

Hence the frequency response characteristics of the filters $H_m(z)$, $m = 0, 1, ..., M-1$ are obtained by uniformly shifting the frequency response of the *prototype* filter by multiples $2\pi/M$, as indicated in Fig. A.2. The M filters $H_m(z)$ defined by Eq. (A.5) can be used as the analysis filters in the analysis filter bank of Fig. A.1(a) or as the synthesis filters in the synthesis filter bank of Fig. A.1(b) [2].

A.2 Polyphase Implementation of Uniform Filter Bank

To develop a computationally efficient filter bank, $H_0(z)$ is expanded as

$$
\begin{aligned}
H_0(z) &= h_0(0) + h_0(1)z^{-1} + h_0(2)z^{-2} + ... \\
&= [h_0(0) + h_0(M)z^{-M} + h_0(2M)z^{-2M} + ...] \\
&\quad + [h_0(1)z^{-1} + h_0(M+1)z^{-(M+1)} + ...] \\
&\quad ... + [h_0(M-1)z^{-(M-1)} + h_0(2M-1)z^{-(2M-1)} + ...] \\
&= \sum_{l=0}^{M-1} z^{-l} \left(\sum_{k=0}^{\infty} h_0(l+kM)z^{-kM} \right)
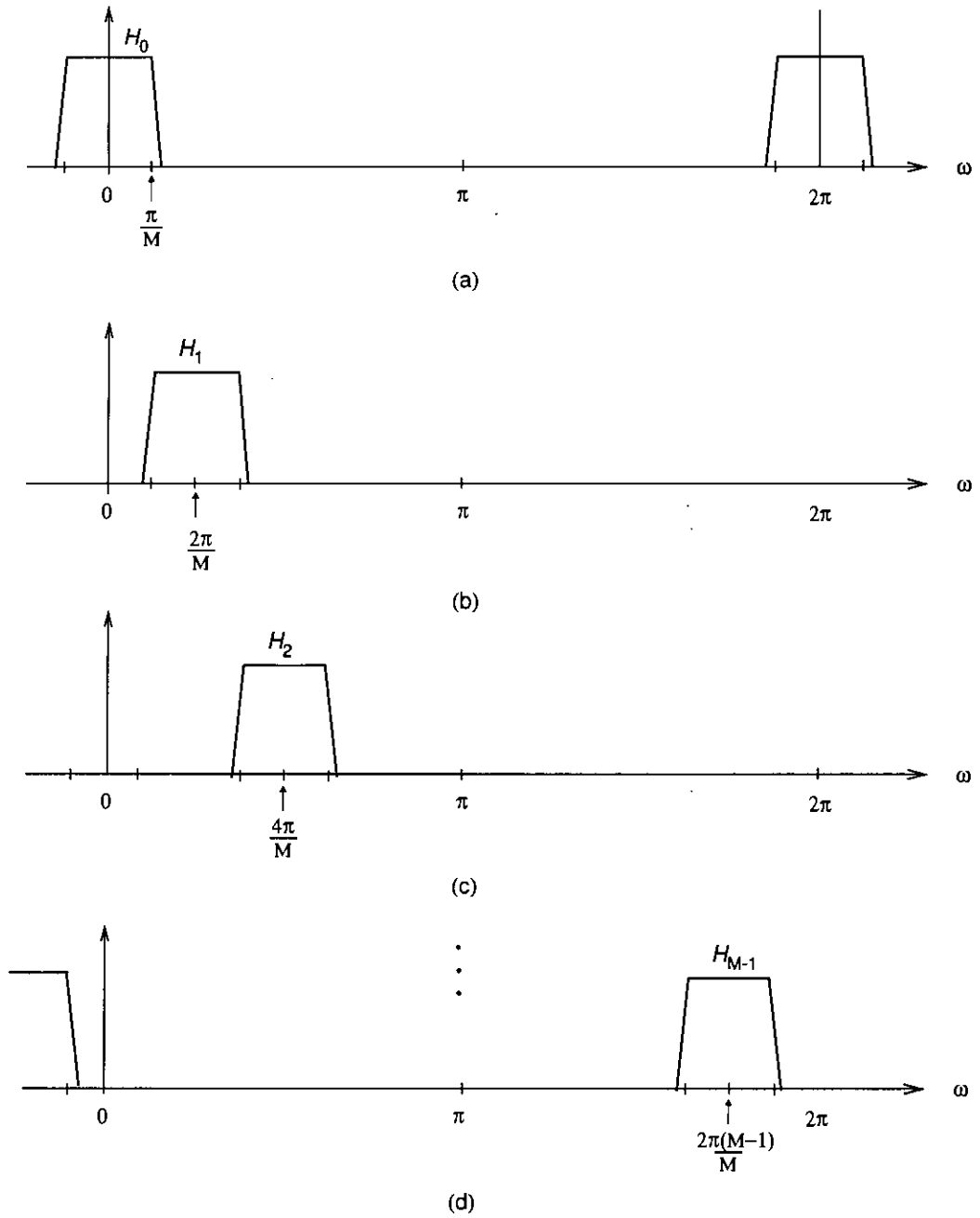\end{aligned}
\qquad \text{(A.7)}
$$

Fig. A.2: The bank of M filters $H_m(z)$ with uniformly shifting frequency responses.

From the above expression

$$H_0(z) = \sum_{l=0}^{M-1} z^{-l} E_l(z^M), \tag{A.8}$$

where $E_l(z)$ is the lth polyphase component of $H_0(z)$:

$$E_l(z) = \sum_{k=0}^{\infty} h_0(l + kM) z^{-k}, \qquad l = 0, 1, ..M - 1. \tag{A.9}$$

Substitution z with zW_M^m in Eq. (A.8) and using the relation $H_m(z) = H_0(zW_M^m)$ of Eq. (A.5)

$$
\begin{aligned}
H_m(z) &= \sum_{l=0}^{M-1} z^{-l} W_M^{-ml} E_l(z^M W_M^{mM}) \\
&= \sum_{l=0}^{M-1} z^{-l} W_M^{-ml} E_l(z^M), \qquad l = 0, 1, ..M - 1, \tag{A.10}
\end{aligned}
$$

using the identity, $W_M^{mM} = 1$. Rewriting Eq. (A.10) in the matrix form, we obtain

$$
\begin{bmatrix} H_m(z) \end{bmatrix} = \begin{bmatrix} 1 & W_M^{-k} & \cdots & W_M^{-(M-1)k} \end{bmatrix}
\begin{bmatrix} E_0(z^M) \\ z^{-1} E_1(z^M) \\ \vdots \\ z^{-(M-1)} E_{M-1}(z^M) \end{bmatrix} \tag{A.11}
$$

Expanding the above Eq. (A.11) gives

$$
\begin{bmatrix} H_0(z) \\ H_1(z) \\ \vdots \\ H_{(M-1)}(z) \end{bmatrix} =
\begin{bmatrix} 1 & 1 & \cdots & 1 \\ 1 & W_M^{-1} & \cdots & W_M^{-(M-1)} \\ \vdots & \vdots & \ddots & \vdots \\ 1 & W_M^{-(M-1)} & \cdots & W_M^{-(M-1)^2} \end{bmatrix}
\begin{bmatrix} E_0(z^M) \\ z^{-1} E_1(z^M) \\ \vdots \\ z^{-(M-1)} E_{M-1}(z^M) \end{bmatrix} \tag{A.12}
$$

which is equivalent to

$$
\begin{bmatrix} H_0(z) \\ H_1(z) \\ \vdots \\ H_{(M-1)}(z) \end{bmatrix} = M\mathbf{D}^{-1}
\begin{bmatrix} E_0(z^M) \\ z^{-1} E_1(z^M) \\ \vdots \\ z^{-(M-1)} E_{M-1}(z^M) \end{bmatrix}, \tag{A.13}
$$

where $\mathbf{D}$ denotes the DFT matrix,

$$
\mathbf{D} = \begin{bmatrix} 1 & 1 & \cdots & 1 \\ 1 & W_M^1 & \cdots & W_M^{(M-1)} \\ \vdots & \vdots & \ddots & \vdots \\ 1 & W_M^{(M-1)} & \cdots & W_M^{(M-1)^2} \end{bmatrix} \tag{A.14}
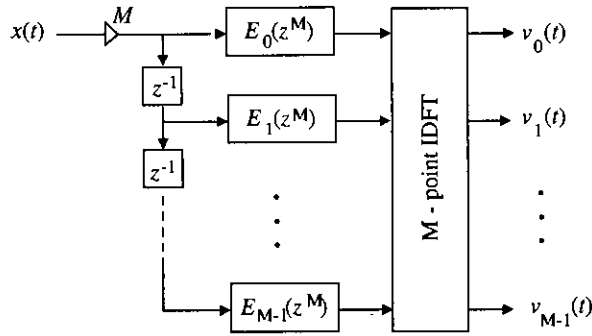$$

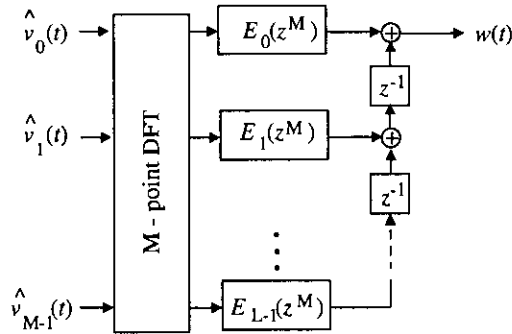Fig. A.3: Polyphase implementation of a uniform analysis filter bank.

Fig. A.4: Polyphase implementation of a uniform synthesis filter bank.

From Eq. (A.13) it is evident that, the uniform filter bank of Fig. A.1(a) can be efficiently implemented by the polyphase decomposition of $H_0(z)$ followed by the DFT as indicated in Fig. A.3. The structure of Fig. A.3 is commonly known as *uniform DFT analysis filter bank.*

By following a similar approach, a structure of Fig. A.4 can be derived, which is commonly known as *uniform DFT synthesis filter bank.*